Supplementary Table 1. Differentially expressed genes common to *Grhl3*^{ct}/J curly tail (CT), RD1 and *VLDLR*$^{-/-}$ (VLDLR) mouse, ranked according to the total fold change.

Probe ID (mouse 430 2.0)	Gene symbol	Gene name	Fold change CT	Adj.P.Val CT	Fold change RD1	Adj.P.Val RD1	Fold change VLDLR	Adj.P.Val VLDLR
1417290_at	Lrg1	leucine-rich alpha-2-glycoprotein 1	91.7636	2.9E-03	14.0924	2.0E-02	54.869	8.9E-03
1418090_at	Plvap	plasmalemma vesicle associated protein	26.6803	1.7E-04	4.04288	1.0E-02	16.1691	2.4E-04
1448550_at	Lbp	lipopolysaccharide binding protein	8.30723	1.0E-02	12.9304	2.2E-03	14.1926	4.4E-03
1438651_a_at	Aplnr	apelin receptor	8.3123	8.6E-04	8.91962	4.0E-04	10.7802	1.4E-04
1428909_at	A130040M12Rik	RIKEN cDNA A130040M12 gene	9.92697	1.5E-03	6.27517	2.5E-03	4.32157	2.9E-02
1417314_at	Cfb	complement factor B	6.26419	5.4E-03	3.70837	1.4E-02	4.7483	2.5E-02
1455396_at	Atp8b1	ATPase, class I, type 8B, member 1	4.06571	3.4E-02	4.83276	1.1E-02	4.81082	4.8E-02
1421813_a_at	Psap	prosaposin	6.34634	4.3E-05	2.39414	3.0E-03	2.42442	8.5E-03
1424374_at	Gimap4	GTPase, IMAP family member 4	2.85718	6.1E-03	3.17947	2.1E-03	3.12492	6.0E-03
1429117_at	Tradd	TNFRSF1A-associated via death domain	2.16031	1.0E-02	2.70536	1.7E-03	2.09701	2.7E-02
1437937_at	Ccbp2	chemokine binding protein 2	2.77401	3.2E-03	1.99412	1.1E-02	2.12383	3.0E-02
1418133_at	Bcl3	B-cell leukemia/lymphoma 3	2.70012	2.9E-03	1.65497	3.6E-02	2.25292	1.5E-02
1423082_at	Derl1	Der1-like domain family, member 1	2.63764	1.5E-03	1.80582	8.7E-03	1.78428	4.1E-02
1420886_a_at	Xbp1	X-box binding protein 1	2.03224	2.4E-03	2.01532	1.6E-03	1.91993	5.5E-03
1422470_at	Bnip3	BCL2/adenovirus E1B interacting protein 3	1.61685	3.5E-02	2.1982	1.9E-03	1.97173	1.3E-02
1451486_at	Slc46a3	solute carrier family 46, member 3	2.09355	9.5E-03	1.72516	1.9E-02	1.91872	3.7E-02
1431146_a_at	Cpne8	copine VIII	1.71393	2.2E-02	1.76654	9.1E-03	2.12126	7.1E-03
1451160_s_at	Pvr	poliovirus receptor	1.63952	4.0E-02	1.81735	9.5E-03	2.07993	1.2E-02
1433954_at	4632419I22Rik	RIKEN cDNA 4632419I22 gene	1.66072	2.7E-02	1.8004	7.2E-03	1.71569	4.8E-02
1418621_at	Rab2a	RAB2A, member RAS oncogene family	1.53365	9.3E-03	1.8329	9.5E-04	1.63074	7.2E-03
1420475_at	Mtpn	myotrophin	1.63782	6.6E-03	1.63484	3.5E-03	1.63386	1.2E-02
1432271_a_at	Dcun1d5	DCN1, defective in cullin neddylation 1, domain containing 5 (S. cerevisiae)	1.38274	3.9E-02	1.69433	2.3E-03	1.53182	2.4E-02
1428090_at	Ptcd3	pentatricopeptide repeat domain 3	1.45038	1.1E-02	1.53833	2.9E-03	1.42394	2.9E-02
1418437_a_at	Mlx	MAX-like protein X	1.31619	4.4E-02	1.69152	1.3E-03	1.38383	5.0E-02
1419104_at	Abhd6	abhydrolase domain containing 6	1.53807	3.5E-03	1.35695	1.0E-02	1.41002	2.3E-02
1460585_x_at	Pisd	phosphatidylserine decarboxylase	1.38932	1.3E-02	1.35054	1.1E-02	1.45259	1.3E-02
1441593_at	---	---	-5.8006	1.5E-02	-20.557	6.7E-04	-9.2821	8.1E-03
1420511_at	Prph2	peripherin 2	-10.884	2.5E-02	-11.855	1.1E-02	-11.918	4.8E-02
1444552_at	---	---	-10.679	2.1E-04	-17.453	6.6E-05	-5.9313	1.1E-03
1441789_at	---	---	-8.173	1.9E-03	-14.935	2.9E-04	-5.5579	8.7E-03
1440068_at	---	---	-5.2199	9.4E-04	-2.2646	1.6E-02	-8.3788	5.2E-05
1446616_at	---	---	-3.3061	6.6E-03	-6.987	3.0E-04	-3.829	5.5E-03
1441671_at	---	---	-3.4247	9.4E-04	-4.639	1.8E-04	-4.8477	5.3E-05

Supplementary Table 1 (continued)

Probe ID (mouse 430 2.0)	Gene symbol	Gene name	Fold change CT	Adj.P.Val CT	Fold change RD1	Adj.P.Val RD1	Fold change VLDLR	Adj.P.Val VLDLR
1445746_at	Eif4h	Eukaryotic translation initiation factor 4H, mRNA (cDNA clone MGC:11689 IMAGE:3962104)	-3.8752	1.9E-03	-4.5091	6.7E-04	-4.4588	7.4E-04
1458068_at	---	---	-3.4222	1.1E-02	-4.9557	1.7E-03	-3.0991	3.7E-02
1447024_at	---	---	-3.5262	5.0E-03	-4.103	1.6E-03	-3.7124	6.5E-03
1457477_at	Mbnl2	muscleblind-like 2	-2.4561	3.9E-02	-5.9534	9.0E-04	-2.9218	4.1E-02
1459687_x_at	---	---	-2.6253	3.2E-02	-5.014	1.6E-03	-3.0497	3.7E-02
1442548_at	---	---	-3.1449	1.2E-02	-3.8378	3.0E-03	-3.3423	1.9E-02
1436892_at	Spred2	sprouty-related, EVH1 domain containing 2	-2.9503	2.4E-03	-4.7226	1.8E-04	-2.6117	6.8E-03
1460567_at	Rfx7	regulatory factor X, 7	-2.8183	5.5E-03	-3.5444	1.3E-03	-3.8806	1.1E-03
1442278_at	Kdm5b	Jumonji, AT rich interactive domain 1B (Rbp2 like) (Jarid1b), mRNA	-3.0173	1.8E-02	-4.1552	3.0E-03	-3.0153	4.1E-02
1429113_at	2900092E17Rik /// Prrt2	RIKEN cDNA 2900092E17 gene /// proline-rich transmembrane protein 2	-3.3018	2.6E-02	-3.1771	1.6E-02	-3.5922	4.4E-02
1442411_at	---	---	-3.1871	6.6E-03	-3.2468	3.2E-03	-2.5439	4.1E-02
1442735_at	---	---	-2.7302	2.0E-02	-3.1033	6.0E-03	-2.7454	4.6E-02
1437965_at	Heatr1	HEAT repeat containing 1	-2.1302	3.1E-02	-3.8366	1.2E-03	-2.5485	2.5E-02
1458798_at	---	---	-2.8396	2.1E-04	-2.7643	1.8E-04	-2.2725	7.4E-04
1444599_at	Herc4	hect domain and RLD 4	-3.2621	9.4E-04	-2.1305	4.6E-03	-2.3084	8.6E-03
1440755_at	---	---	-2.1872	1.1E-02	-2.8937	1.6E-03	-2.1518	2.7E-02
1446954_at	---	---	-2.1791	8.6E-04	-2.5859	1.8E-04	-2.4363	1.1E-04
1435984_at	Zfp40	Zinc finger protein 40 (Zfp40), mRNA	-2.0125	1.4E-02	-1.7045	2.6E-02	-3.0637	1.1E-03
1426287_at	Atxn7	ataxin 7	-1.8399	1.0E-02	-2.1381	2.0E-03	-1.9469	1.2E-02
1419236_at	Helb	helicase (DNA) B	-1.6318	1.2E-02	-2.4282	3.8E-04	-1.7659	1.1E-02
1428996_at	4833426J09Rik	RIKEN cDNA 4833426J09 gene	-1.823	3.2E-02	-1.6059	4.7E-02	-2.361	1.0E-02
1432978_at	9030607L02Rik	RIKEN cDNA 9030607L02 gene	-2.0972	3.5E-03	-1.8484	4.8E-03	-1.823	2.2E-02
1442071_at	Abce1	ATP-binding cassette, sub-family E (OABP), member 1	-1.7106	1.4E-02	-2.3357	9.3E-04	-1.6402	4.9E-02
1445438_at	Ddhd1	DDHD domain containing 1	-1.7985	6.8E-03	-2.1305	1.2E-03	-1.6959	2.3E-02
1445436_at	BC059842	PREDICTED: Mus musculus cDNA sequence BC059842 (BC059842), mRNA	-2.0196	1.8E-03	-1.9107	1.6E-03	-1.6305	2.3E-02
1455611_at	Pias1	protein inhibitor of activated STAT 1	-1.8771	1.8E-03	-1.453	1.2E-02	-1.6163	1.3E-02
1440331_at	Kdsr	3-ketodihydrosphingosine reductase	-1.6376	3.1E-03	-1.4473	6.7E-03	-1.4862	1.9E-02
1442443_at	---	---	-1.4444	2.4E-02	-1.5212	6.7E-03	-1.5421	2.3E-02
1437919_at	Bdp1	B double prime 1, subunit of RNA polymerase III transcription initiation factor IIIB	-1.4457	1.1E-02	-1.495	3.7E-03	-1.3805	4.7E-02

Supplementary Table 2. Primer sequences.

Application	Primer name	Primer sequence
Quantitative PCR primers	mLrg1_For	CCATGTCAGTGTGCAGATTC
	mLrg1_Rev	AAGAGTGAGAGGTGGAAGAG
	mTGFβ1_For	TTGCTTCAGCTCCACAGAGA
	mTGFβ1_Rev	TGGTTGTAGAGGGCAAGGAC
	PAI1_ For	CCTCTTCCACAAGTCTGATGGC
	PAI1_Rev	GCAGTTCCACAACGTCATACTCG
	ID1_For	TGAACGGCGAGATCAGTGCCTT
	ID1_Rev	GTGGCTGCGGTAGTGTCTTTC
	mVEGF_For	GACTTGTGTTGGGAGGAGGA
	mVEGF_Rev	TCTGGAAGTGAGCCAATGTG
	mAplin_For	GGCCTTCTCCGTCTTTGTCG
	mAplin_Rev	CCCTCTTGTGCTTCTATCTCTCC
	mAPLNR_For	GGGAGTAAGTTTGGGAAAGAG
	mAPLNR_Rev	TGGAATATGTCTTGTCCTTGG
	mPlGF_For	TTCTCAGGATGTGCTCTGTGAA
	mPlGF_Rev	CTGGTTACCTCCGGGAAATGAC
	GAPDH_For	ACTGAGGACCAGGTTGTCTCC
	GAPDH_Rev	CTGTAGCCGTATTCATTGTCATACC
Genotyping primers	TUF	TGCACCTCTCGAGCAATCG
	TUR	AGAGCATTGCGGGTCAGATC
	NeoFwd	TCATTCTCAGTATTGTTTTGCC
	SD	GACCCCTGAAACAGACGTG
	SU	TCCTGGTGGGAGAGGACTC
	LacInZRev	GTCTGTCCTAGCTTCCTCACTG
Primers for cloning rhLrg1	Lrg1-His_For	GTGTAAGCTTGCCACCATGGCCATGTCCTCTTGGAGCAGAC
	Lrg1-His_Rev	GTGTCTCGAGTCATCACTAGTGATGATGATGGTGATGCTGGGACTTGGCCACTGCCA
Primers for cloning Lrg1-HA	HLRG1For	GTGTAAGCTTGCCACCATGGCCATGTCCTCTTGGAGCAGAC
	HLRG1Rev	GTGTCTCGAGCTGGGACTTGGCCACTGCCA
	nucleotide sequence for 3XHA	GTGTCTCGAGGAGTACCCATACGACGTACCAGATTACGCTTACCCATA CGATGTTCCAGATTACGCTTATCCATATGACGTCCCAGACTATGCCTAG TGATAACTCGAGGTGT
Primers for generating RNA in situ hybridisation probe	mLrg1_insitu_For	CTGGTCGCCAACCGAAACAAGA
	mLrg1_insitu_Rev	AGTCAGCCTAGGAGCCGTTTT

Supplementary Table 2. Primer sequences (continued).

Application	Primer name	Primer sequence
Primers for constructing TGFβ Receptors extracellular domain	ALK1_For	GTGTAAGCTTGCCACCATGGCCATGACCT TGGGCTCCCC
	ALK1_Rev	GTGTGAATTCCTGGCCATCTGTTCCCGGCT
	ALK5_For	GTGTAAGCTTGCCACCATGGCCATGGAGGCGGCGGTCGCT
	ALK5_Rev	GTGTGAATTCCAGTTCCACAGGACCAAGGCC
	TβRII_For	GTGTAAGCTTGCCACCATGGCCATGGGTCGGGGGCTGCT
	TβRII_Rev	GTGTGAATTCTTATCACTACAGGTCCTCCTCTGAGATCAGCTTCTGCTCTTCTGAGAAGATGATGTTGTCATTG
	ENG_For	GTGTAAGCTTGCCACCATGGGCATGGACCGCGGCACGCTCCCT
	ENG_Rev	GTGTGAATTCTTATCACTACGTAGAATCGAGACCGAGGAGAGGGTTAGGGATAGGCTTACCGCCTTTGCTTGTGCAACCAGA
Primers for cloning GST-ENG	ENGpGEXFor	GTGTGGATCCATGGACCGCGGCACGCTCC
	ENGpGEXRev	GTGTGTCGACTTATCACTAGCCTTTGCTTGTGCAACCAGA

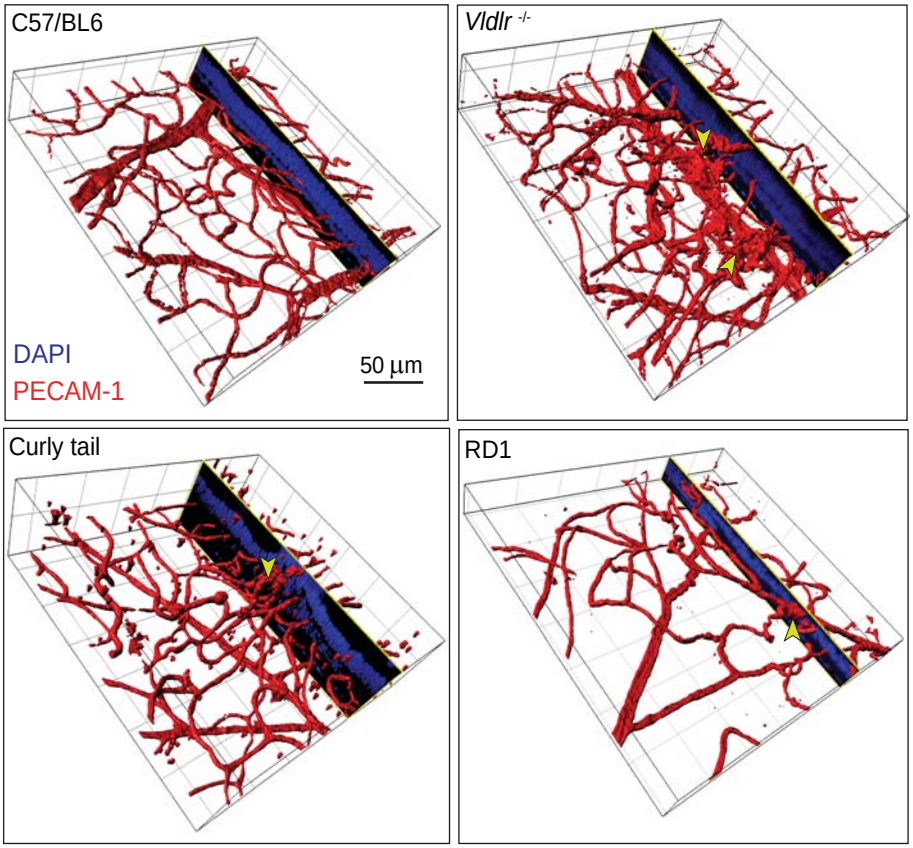

Supplementary Figure 1. Retinal vasculature of C57/BL6 wild type mouse and three mouse models of retinal disease. Imaris rendered representative 3D images of PECAM-1 stained retinal vasculature (red) of control C57/BL6 mouse and of the vascular abnormalities (highlighted by arrow heads) in *Vldlr*$^{-/-}$, Curly tail (*Grhl3*^{ct}/J) and RD1 mice. In each image a single X-Y section stained for nuclei (blue) is incorporated to show the relative positioning of the nuclear layers (see also Supplementary movies 1-4).

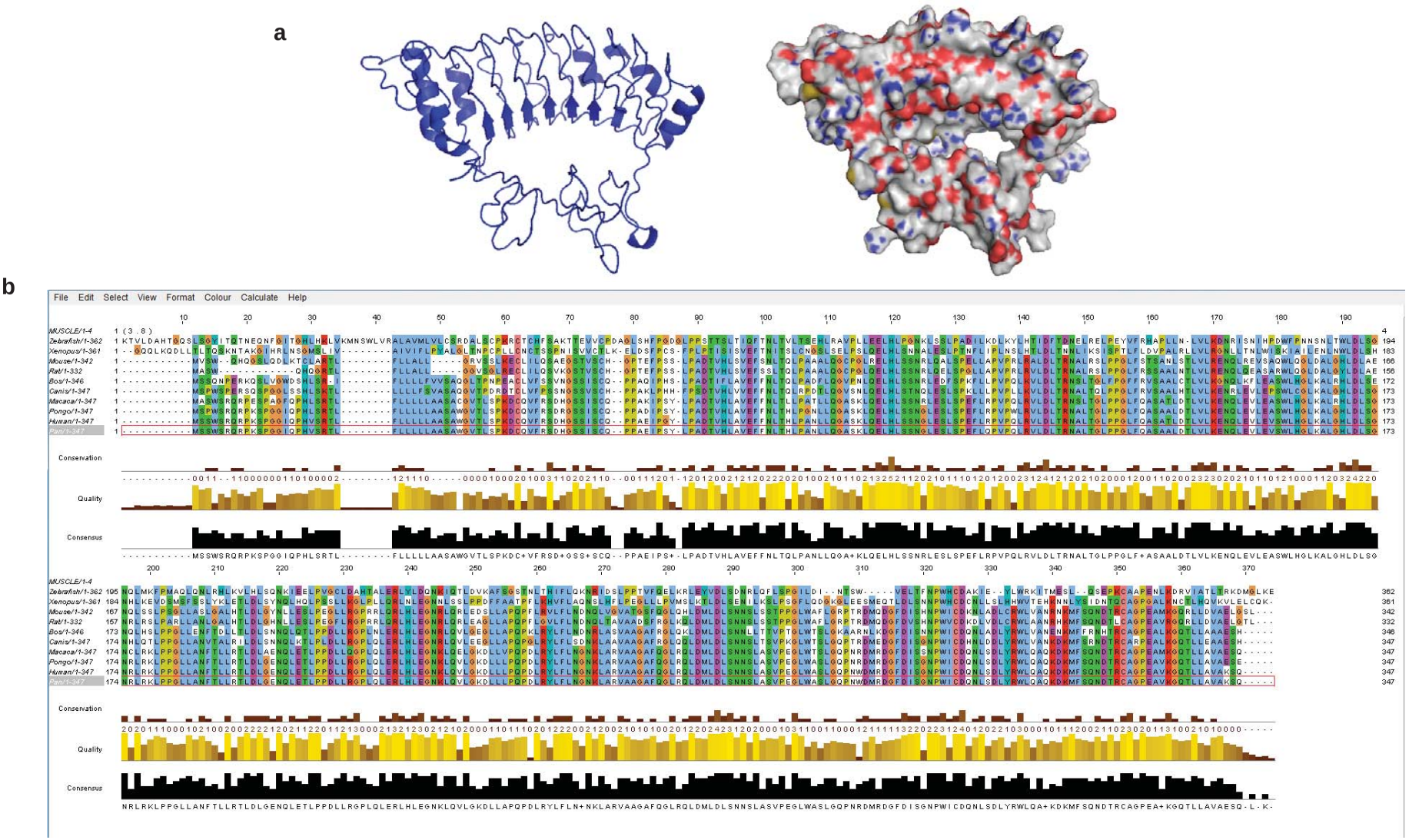

Supplementary Figure 2. Predicted structure and species homology of LRG1. a, Predicted ribbon structure (left) and space-filling model (right) of mouse LRG1 (342 amino acids) obtained through the Robetta full-chain protein structure prediction server (http://robetta.bakerlab.org). The leucine-rich C-terminal (LRC) contains mainly β strands and is connected to the leucine-rich repeats (LRR) by loops. Each LRR contains a β strand and an α helix with the structural units arranged in parallel with a curved β sheet lining the inner circumference and the α helices flanking the outer circumference. The LRC and LRR domain contain 3 potential glycosylation sites with a further 4 sites in the linker region between the LRR and the signal peptide. Images generated courtesy of Professor C.M. Marson (UCL, London). **b**, Alignment of the Lrg1 amino-acid sequence between different vertebrate species obtained through the EMBL-EBI European Bioinformatics Institute.

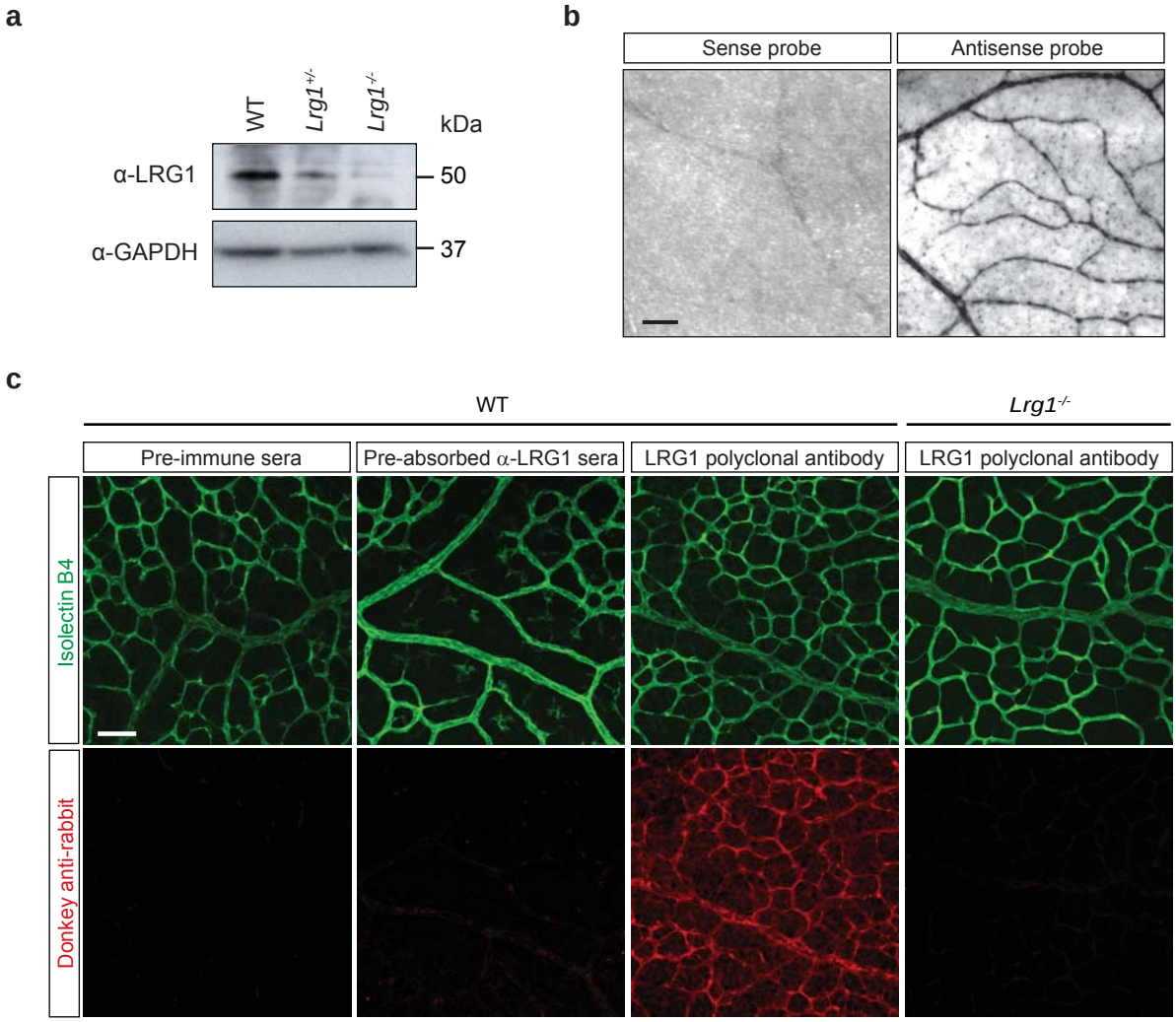

Supplementary Figure 3. Specificity of Lrg1 probes and antisera. a, Rabbit anti-LRG1 polyclonal antibody western blot of retinal cell lysates from wild type (WT), heterozygous (*Lrg1*$^{-/+}$) and homozygous (*Lrg1*$^{-/-}$) mice (3 months old) showing loss of LRG1 signal in the latter. **b**, *In situ* hybridisation of *Lrg1* sense and antisense probes in P35 flat-mounted mouse retinae showing positive signal in antisense image. **c**, Flat-mounted WT and *Lrg1*$^{-/-}$ retinae stained for vessels (isolectin B4; green) and with pre-immune rabbit sera, pre-absorbed rabbit anti-LRG1 sera and affinity purified rabbit polyclonal anti-LRG1 antibody. Staining with pre-immune rabbit sera and pre-absorbed rabbit sera in WT mice and affinity purified rabbit polyclonal anti-LRG1 antibody in *Lrg1*$^{-/-}$ mice give a negative signal. Scale bar 50μm.

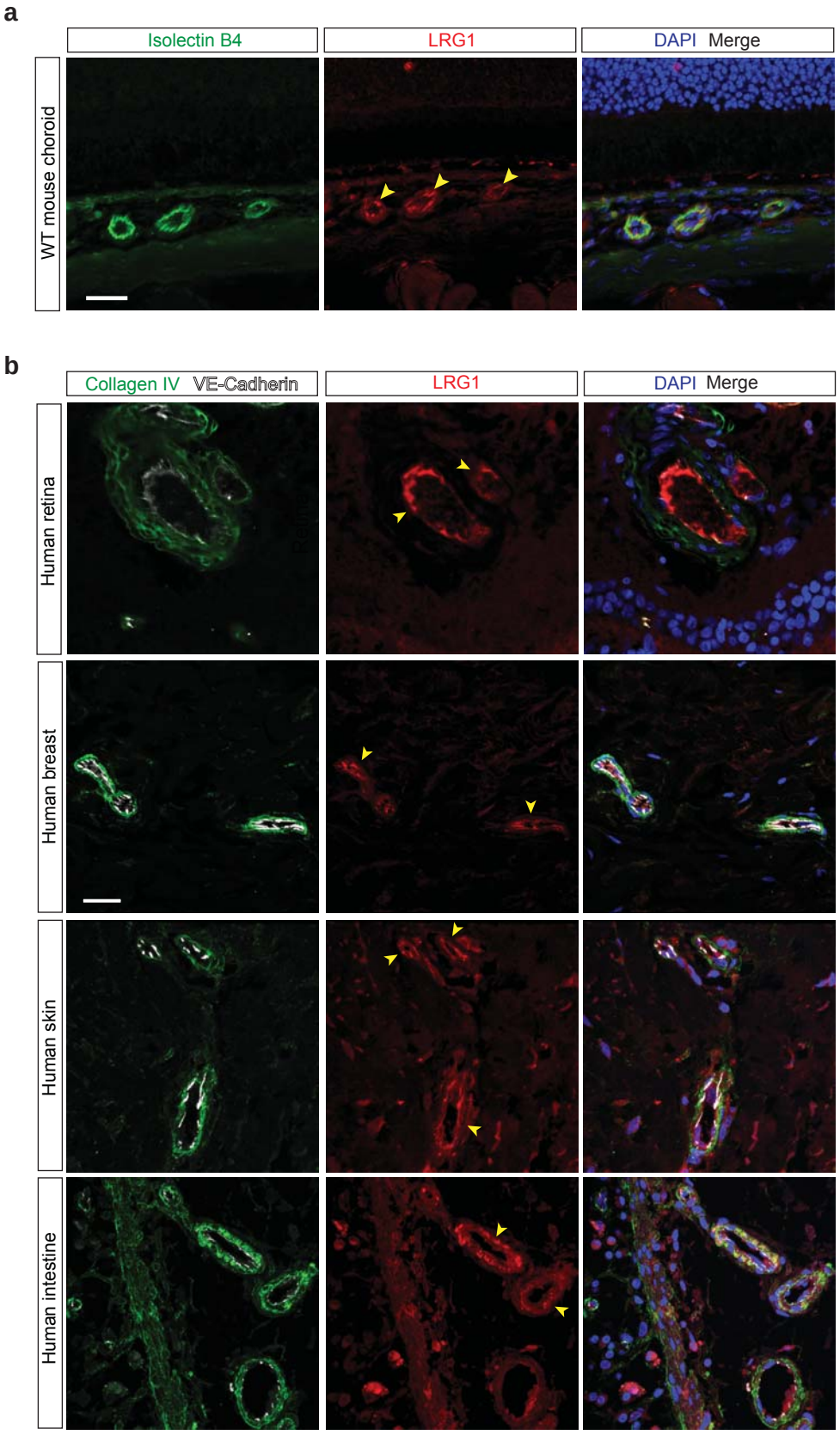

Supplementary Figure 4. LRG1 is expressed in the vasculature of other tissues. a, Mouse section of outer retina and choroid showing staining of the choroidal vasculature with isolectin B4 (green), LRG1 (red) and nuclei (blue). LRG1 is expressed primarily in the choroidal vessels. Scale bar 20μm. **b**, Human retina, breast, skin and intestine stained with antibodies against collagen IV (green), VE-cadherin (white), LRG1 (red) and nuclei (blue) shows LRG1 non-exclusive expression with the vasculature. Scale bar 20μm.

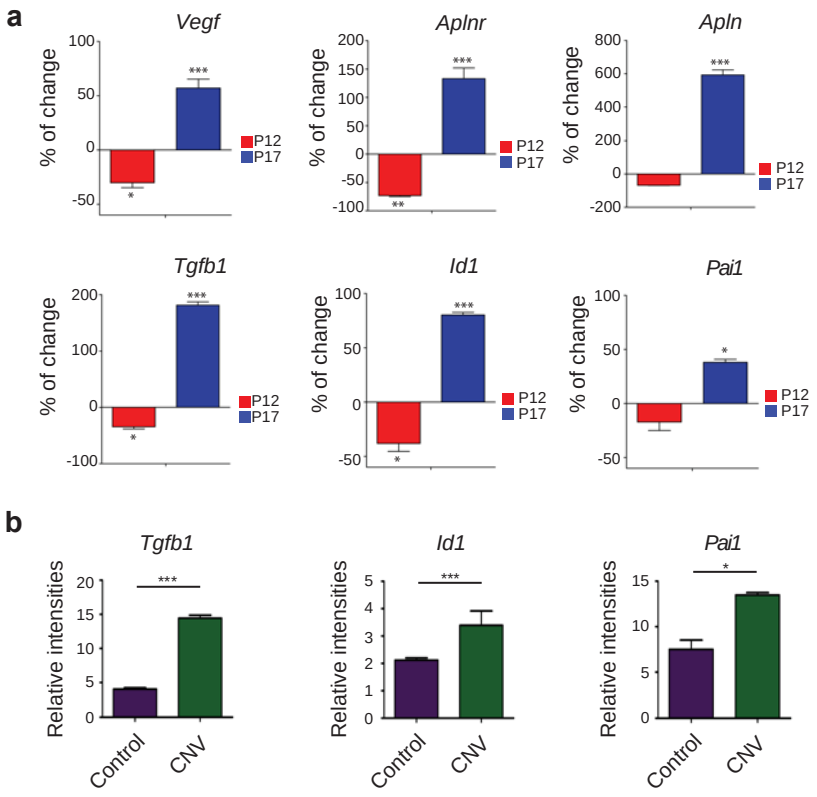

Supplementary Figure 5. Expression of angiogenic/TGFβ related genes in the retina of OIR and CNV mice. a, Quantitative RT PCR analysis of the expression of angiogenic/TGFß related genes in the retina of OIR mice at P12 and P17. Hypoxic-responsive genes *Vegfa* , *Aplnr* and its ligand *Apln* are reduced during the hyperoxic phase (P12) and significantly enhanced at P17 when the maximal neovascular response is observed. *Tgfb1* gene expression and the AKL1-Smad 1/5/8 pathway induced gene *Id1* are also reduced at P12 and enhanced at P17. The ALK5-Smad 2/3 pathway induced gene *Pai1* is up-regulated at P17. **b**, In the retina of laser induced CNV 7 days post-induction, *Tgfb1, Id1* and *Pai1* gene expression is significantly up-regulated compared to untreated age-matched WT C57Bl/6 control mice. **P*<0.05; ***P*<0.01; ****P*<0.001; *n* = 3.

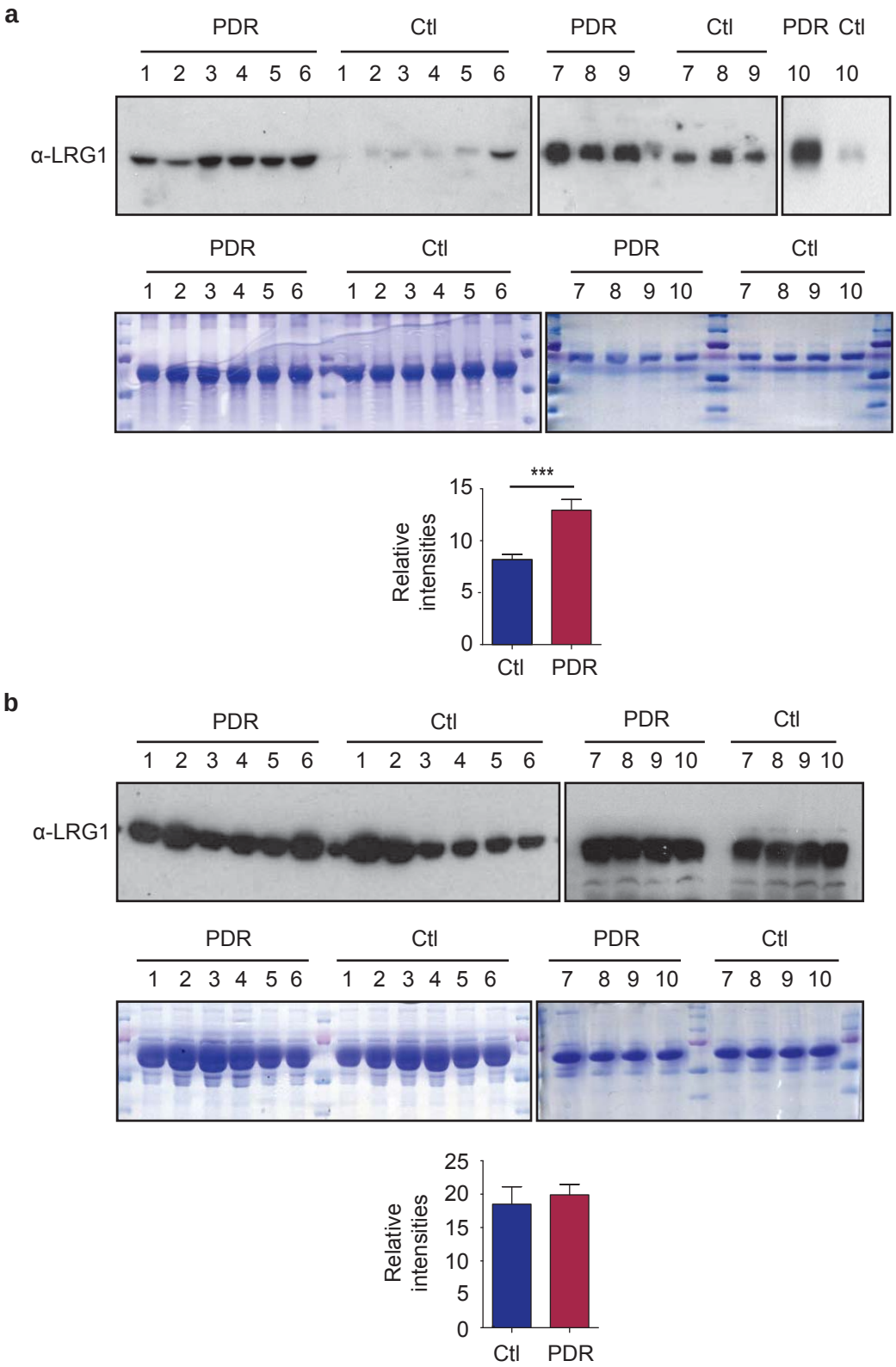

Supplementary Figure 6. LRG1 protein levels are elevated in the vitreous of proliferative diabetic retinopathy patients. a, Western blots of vitreal LRG1 from ten human subjects with proliferative diabetic retinopathy (PDR) and ten non-PDR controls (with idiopathic epiretinal membranes). Quantitative analysis shows a significant increase in PDR patients (***P<0.001). **b**, No significant difference in plasma LRG1 protein level was observed between PDR and non-PDR controls. Total vitreous/plasma protein was normalized before western blotting as shown by Coomassie blue staining of the SDS-PAGE gel. The LRG1 protein level was quantified by densitometry and normalised against the total protein in vitreous /plasma using Image J. All values represent means ± s.e.m. Significance determined by Student's t-test (***P<0.001).

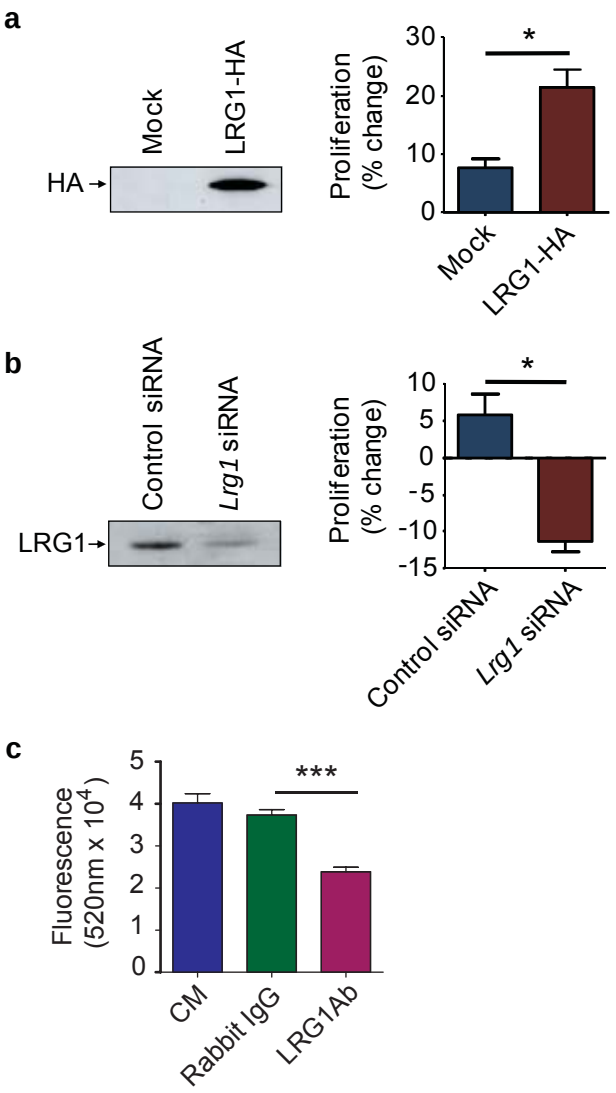

Supplementary Figure 7. LRG1 contributes to endothelial cell proliferation and migration. a, Western blot analysis showing over-expression of hLRG1-HA (using anti-HA antibody) in conditioned media from hLRG1-HA transfected GPNT brain endothelial cells. The GPNT cells transfected with the human *LRG1* gene exhibit enhanced cell proliferation after 3 h in the presence of 5ng/ml TGFβ1 (as determined by Ki67 staining) compared to mock-treated controls. **b,** Western blot showing decrease in expression of LRG1 in conditioned media from *Lrg1* siRNA treated GPNT cells compared to control siRNA-treated controls. Following 5ng/ml TGFβ1 treatment, there is a reduction in cell proliferation in *Lrg1* siRNA treated GPNT cells. (**P*<0.05; *n*=3). **c,** HUVEC migration through a porous membrane (Transwell migration assay) over 24 hours was inhibited following addition of an anti-LRG1 polyclonal antibody compared to pre-immune rabbit IgG (CM = complete media). Cells that migrated through the Transwell were harvested and lysed in lysis buffer, and then labelled with CyQuant GR Dye for fluorescence measurement at 520nm. (****P*<0.001; *n*=3).

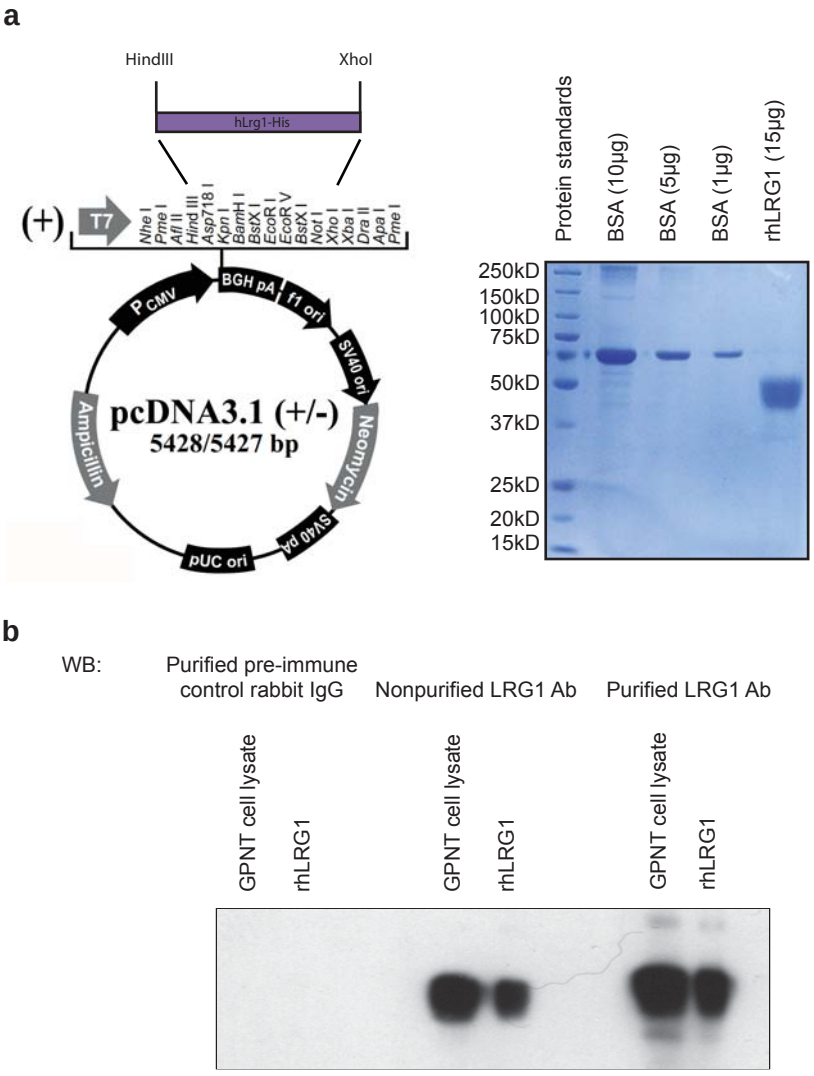

Supplementary Figure 8. Generation of recombinant human LRG1 protein (rhLRG1) and purified rabbit anti-hLRG1 polyclonal antibody. a, Schematic outline of the rhLRG1 cloning strategy. The coding sequence of human *LRG1* mRNA (NM_052972) carrying a Kozak consensus sequence at the 5' end and a 6 x His tag at the 3' end was cloned into pcDNA3.1 expression vector at the HindIII/XhoI sites to form pcDNA-rh*LRG1*-His. Right, purified rhLRG1 protein was analysed by a Coomassie blue stained gel. **b**, The specificity of LRG1 polyclonal antibody (CD10-52) was tested by western blot to detect LRG1 expression in GPNT cell lysate with recombinant human LRG1 as a positive control. Purified pre-immune rabbit IgG was used as a negative control of CD10-52.

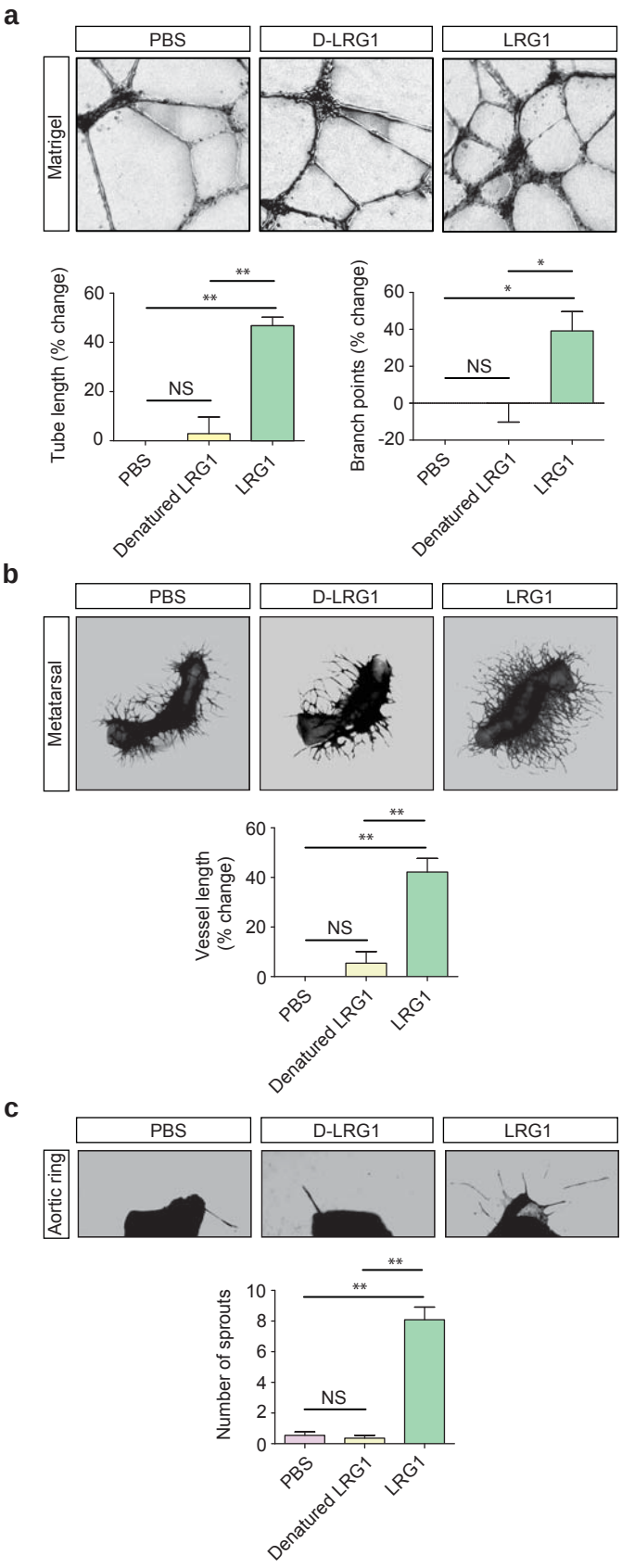

Supplementary Figure 9. PBS vehicle control versus denatured LRG1 protein control. Phosphate-buffered saline (PBS) vehicle-treated and denatured protein control-treated HUVEC in the Matrigel tube formation assay exhibit similar endothelial tube formation (n ≥ 9 from three independent assays). **b**, PBS and denatured protein control-treated metatarsals (n ≥ 30 from three independent assays) and **c**, aortic rings (n ≥ 15 from three independent assays) also exhibit similar vessel formation. Data given as mean ± s.e.m. Significance determined by Student's t-test (*P<0.05; **P<0.01).

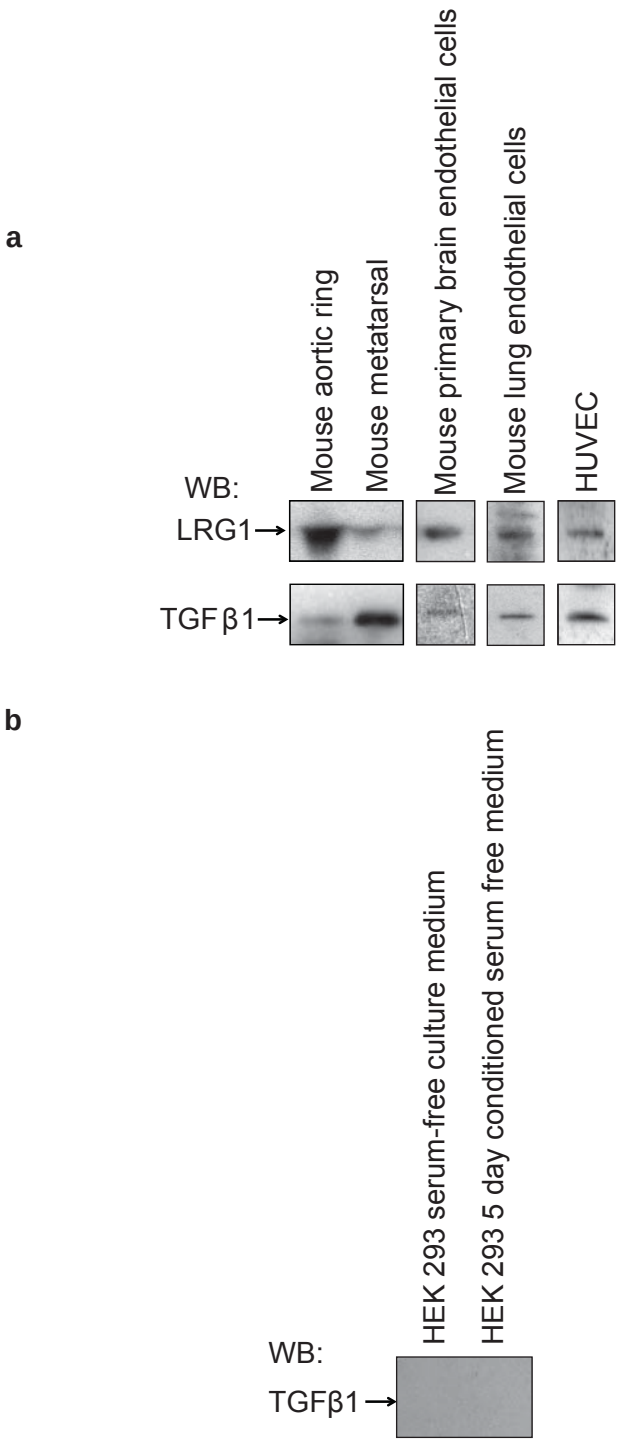

Supplementary Figure 10. LRG1 and TGFß-1 expression in conditioned media. a, Western blot analysis showing the presence of LRG1 and TGFß-1 in conditioned media harvested from mouse aortic ring, mouse metatarsal, mouse primary brain endothelial cell cultures, immortalised mouse lung endothelial cell cultures (from *Rosa26-CreERT:Eng*$^{fl/fl}$ mouse) and HUVEC Matrigel assays. **b**, Western blot analysis showing the absence of TGFß-1 in HEK 293 cell culture medium and following 5 days of cell conditioning.

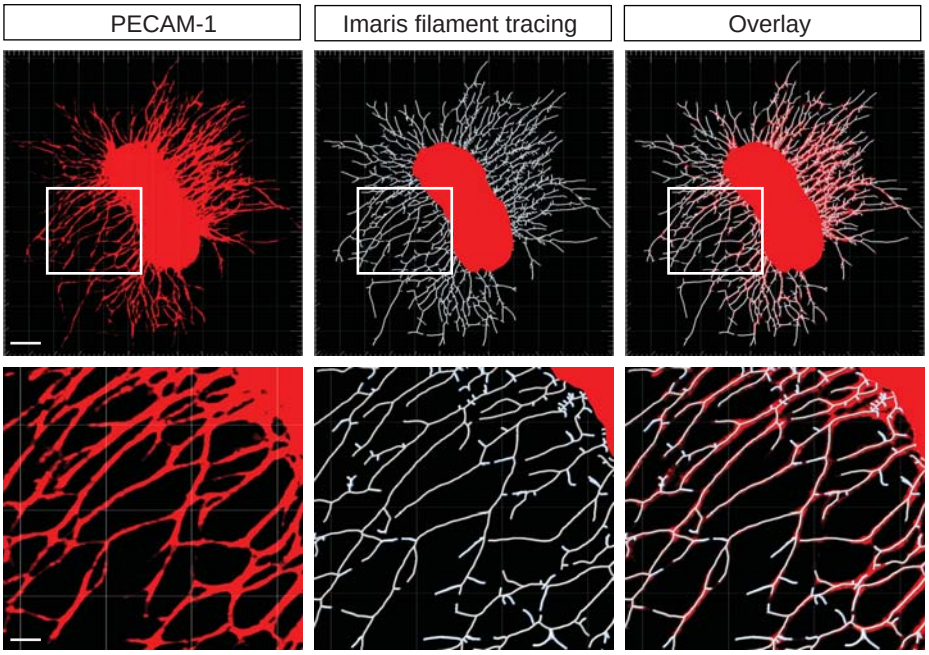

Supplementary Figure 11. Metatarsal angiogenesis assay vessel quantification. Example of image rendering for quantification of vascular growth in the metatarsal angiogenesis assay. Metatarsal vessel outgrowth stained with anti-PECAM-1 antibody (red) is captured digitally, and after thresholding vessel configuration quantified (white) using Imaris filament tracing image analysis software (Bitplane AG, Switzerland).

a

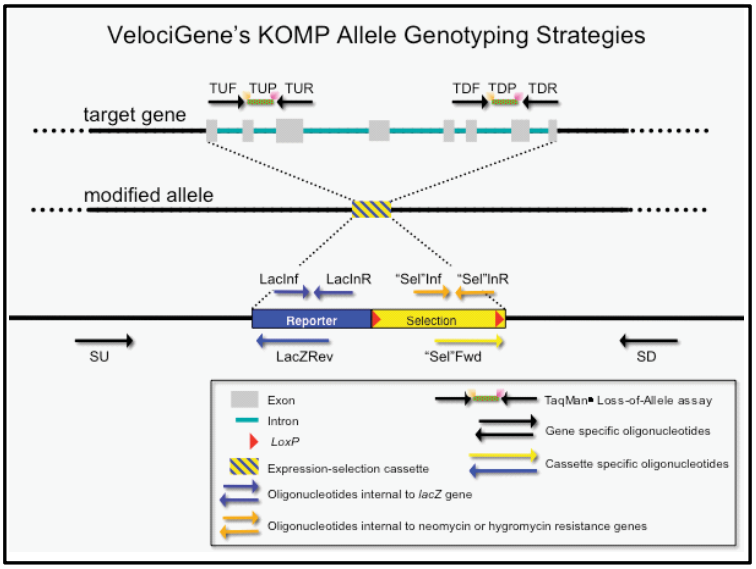

b

Forward Primer	Reverse Primer	Length	WT	HET	KO
SU	LacZRev	367 bp	-	+	+
TUF	TUR	76 bp	+	+	-
NeoFwd	SD	307 bp	-	+	+

c

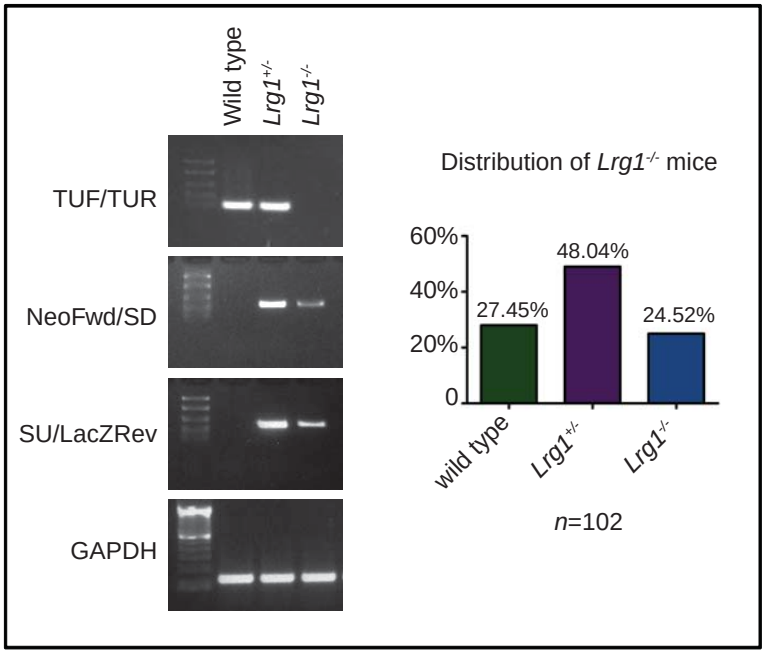

Supplementary Figure 12. Genotyping the *Lrg1*$^{-/-}$ mouse. a, Strategy for PCR-based genotyping Lrg1 knockout mice (from KOMP). **b**, The sizes of expected PCR products for wild type (WT), heterozygote (HET) and null mutant (KO). **c**. Genotyping examples of WT, heterozygous and homozygous mice and their ratio in the progeny of heterozygous breeding pairs.

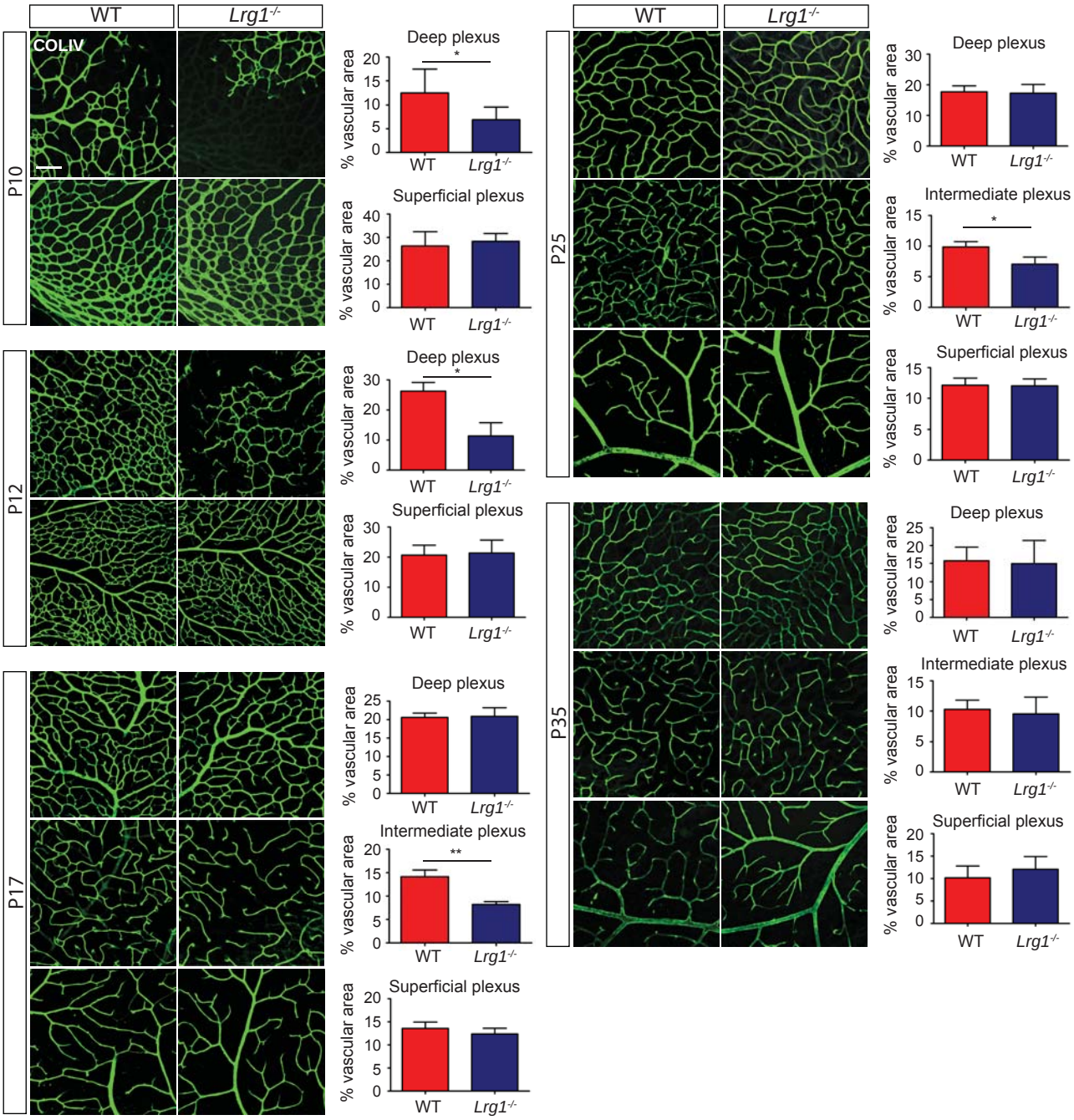

Supplementary Figure 13. Retinal vascular development in the *Lrg1*$^{-/-}$ mouse. Retinal blood vessels were visualized in retinal flat-mounts using an anti-collagen IV antibody followed by FITC-conjugated secondary and imaged using a confocal scanning laser microscope. Z-sections were captured and analysed from the central and peripheral retina (four regions per retina each of 0.4mm^2) to reveal the inner, intermediate and deep vascular plexuses of the C57/Bl6 wild type (WT) and *Lrg1*$^{-/-}$ mouse (*n* = 6 for each group). Vascularization of the retina is delayed in *Lrg1*$^{-/-}$ mice compared to that in WT littermate controls at P10, P12, P17 and P25. The P35 retinal vasculature in the *Lrg1*$^{-/-}$ mice shows no difference compared to that from WT. Significance determined by Student's t-test (**P*<0.05; ***P*<0.01). Scale bar = 40μm.

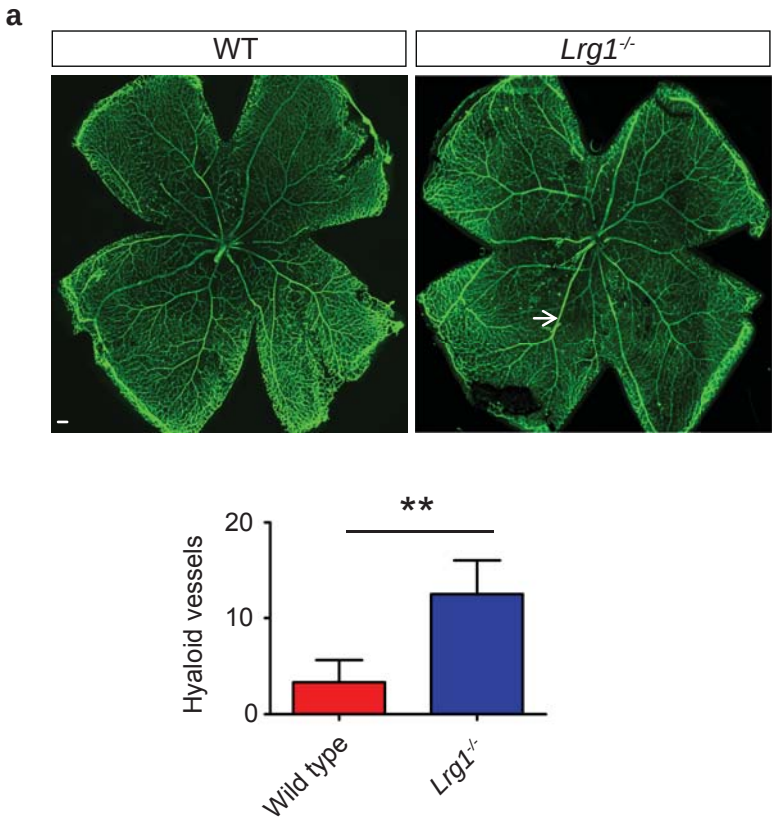

Supplementary Figure 14. Hyaloid vessels persist in the *Lrg1*$^{-/-}$ mouse. a, Wild type **(**WT) flat mounted retina stained for the vasculature (anti-collagen IV) show regression of the hyaloid vasculature at P35. In the *Lrg1*$^{-/-}$ mouse retina persistent hyaloid vessels (arrow) at P35 can be observed. Only primary radial hyaloid vessels were enumerated (n=30 for each group). Scale bar = 68μm. **b**, Following 3D rendering persistent hyaloid vessels (green) are seen integrating into the superficial retina to give rise to anastomosis with the retinal vasculature (*n*=30 for each group). Significance determined by Student's t-test (**P<0.01).

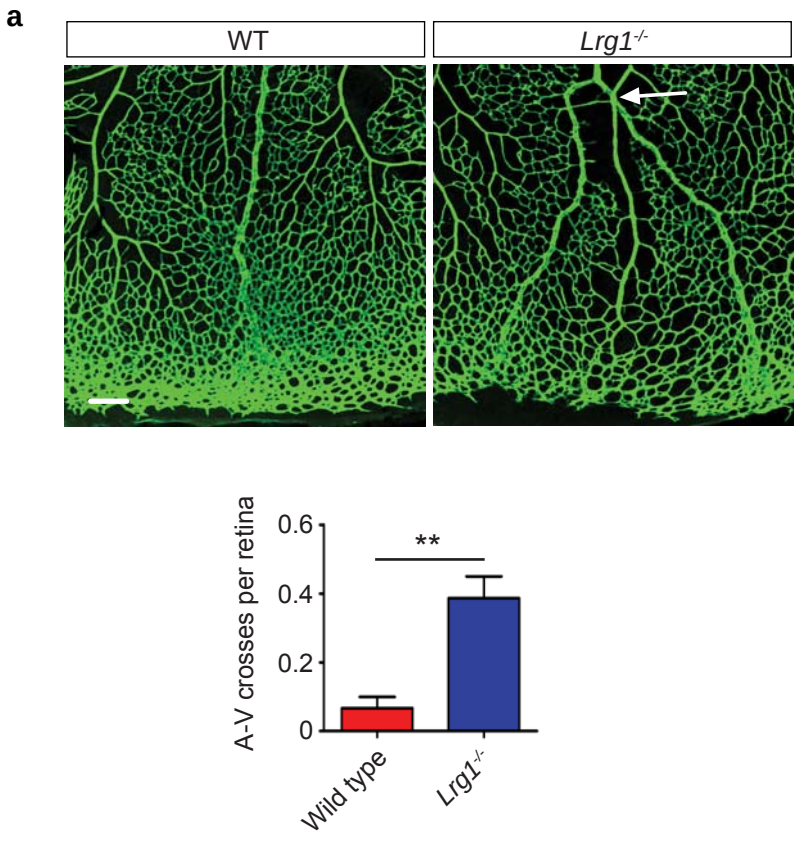

Supplementary Figure 15. Increased arteriovenous crossing in the *Lrg1*$^{-/-}$ mouse. a, At P10 the wild type (WT) retina shows a regular alternating pattern of arteries and veins. At the same developmental stage *Lrg1*$^{-/-}$ mice exhibit an approximate 5-fold increase in the frequency of arteriovenous crossovers within the inner superficial vascular plexus (white arrow). **b**, 3D Imaris rendering shows close apposition and possible anastomosis between the crossing arteries and veins (*n*=30 for each group). Significance determined by Student's t-test (**P<0.01). Scale bar 120μm.

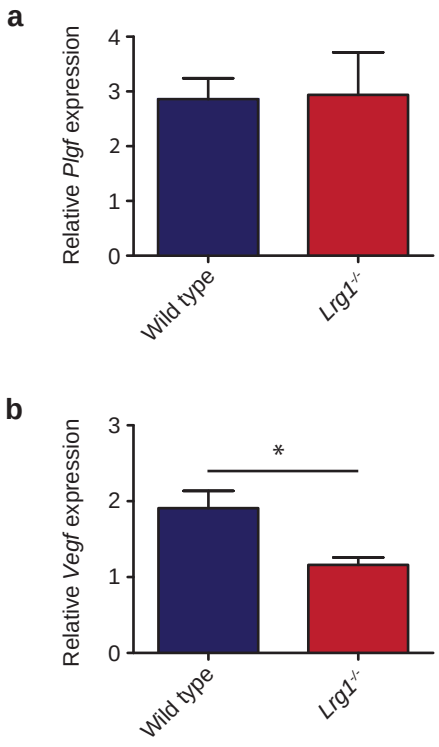

Supplementary Figure 16. *Plgf* and *Vegfa* gene expression in *Lrg1*$^{-/-}$ mice. Quantitative RT PCR analysis of **a,** *Plgf* mRNA expression in the retina of 3 month old WT and *Lrg1*$^{-/-}$ mice relative to *Gapdh* (*n*=4). **b**, *Vegfa* expression in the retina of 3 month old WT and *Lrg1*$^{-/-}$ mice relative to *Gapdh* (*n*=4). Significance determined by Student's t-test (**P*<0.05).

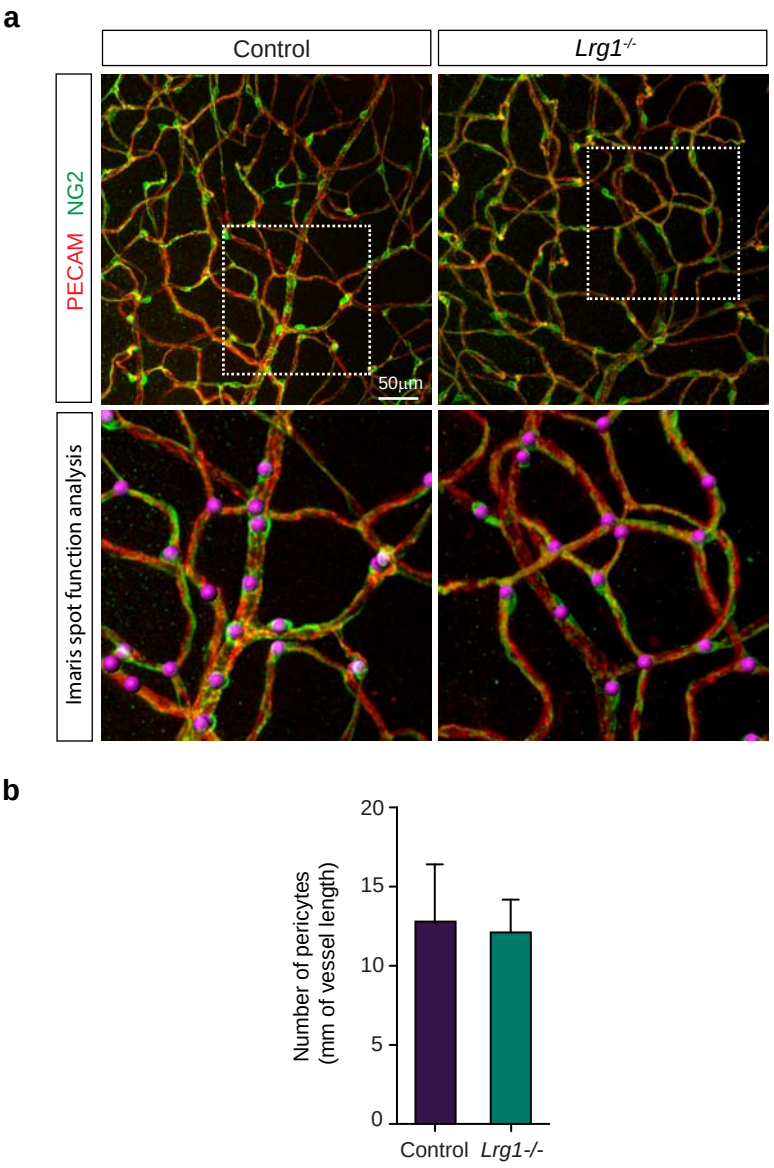

Supplementary Figure 17. Pericyte coverage is identical in WT and *Lrg1*$^{-/-}$ mice. a, Representative confocal images of retinal vasculature (upper panels) from WT (*n*=3) and *Lrg1*$^{-/-}$ (*n*=3) mice stained for PECAM-1 (red) and NG2 (green). Lower panels depict pericyte detection using the spot function (magenta spots) in Imaris software of white boxed area from upper images. **b**, Histogram showing average number of pericytes per mm of vessel length. No significant difference was observed (Student's t-test).

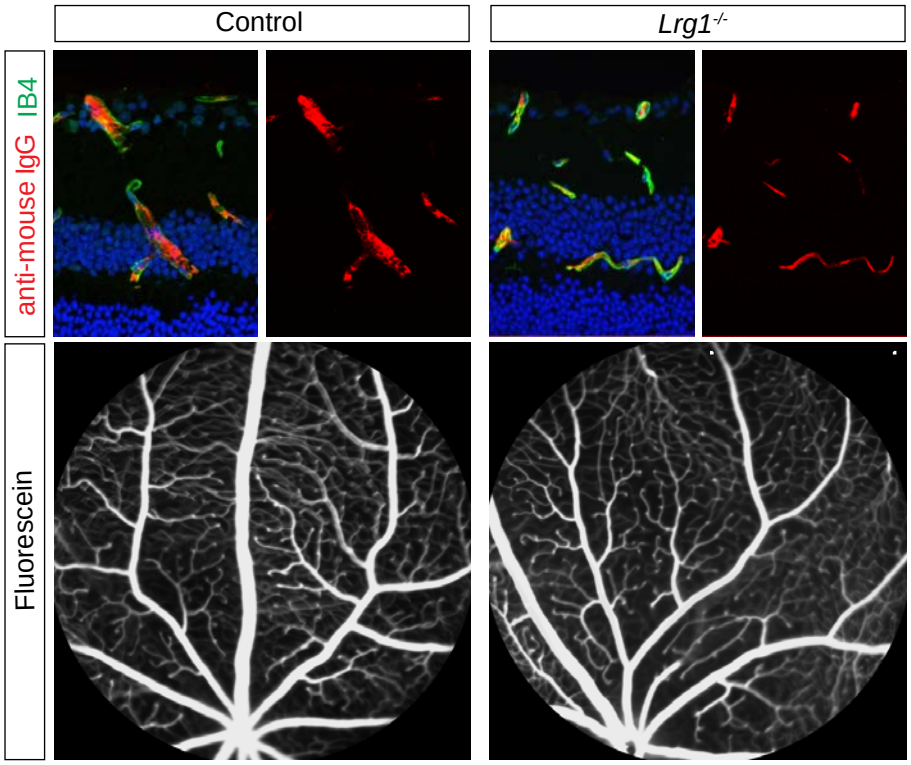

Supplementary Figure 18. Retinal vascular barrier properties are retained in the *Lrg1*$^{-/-}$ mouse. Upper panels show staining of representative retinal sections for blood vessels (isolectin B4 - green), mouse IgG (Ab 594 - red) and nuclei (DAPI - blue). IgG is retained within the vascular compartment in control (left) and *Lrg1*$^{-/-}$ mice (right; *n*=3 animals for each group) indicating retention of blood-retinal barrier properties. The lower panels show representative fluorescein angiographs from control (left) and *Lrg1*$^{-/-}$ mice (right; *n*=3 animals for each group) at late phase (8 minutes) post fluorescein injection showing an absence of fluorescein leakage from the blood and hence maintenance of an intact blood-retinal barrier in the latter.

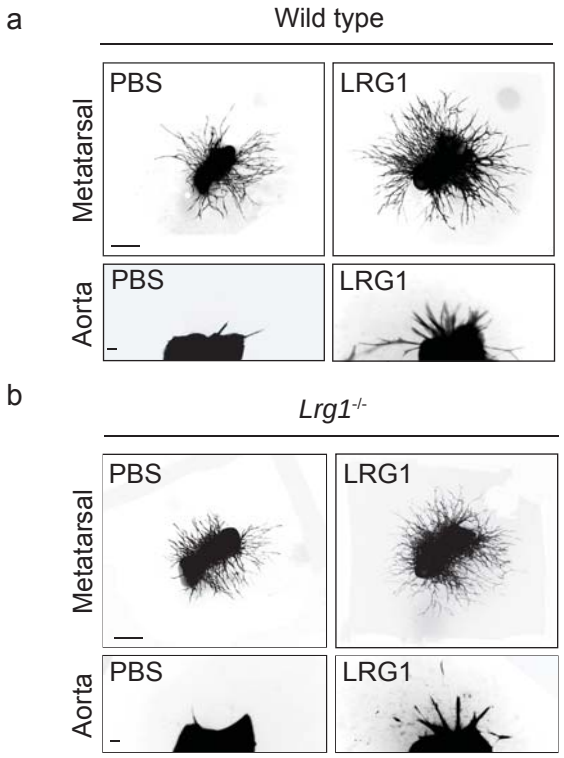

Supplementary Figure 19. LRG1 promotes angiogenesis in WT mice and rescues angiogenesis in *Lrg1*$^{-/-}$ mice. a, Examples of vessel outgrowth in the metatarsal (top row) and aortic ring (bottom row) assay showing enhanced angiogenesis following LRG1 treatment. **b,** Examples of vessel outgrowth in metatarsals (top row) and aortic rings (bottom row) from *Lrg1*$^{-/-}$ mice showing rescue of LRG1 induced angiogenesis. See Figure 2 for quantification. Scale bar = 1,500μm.

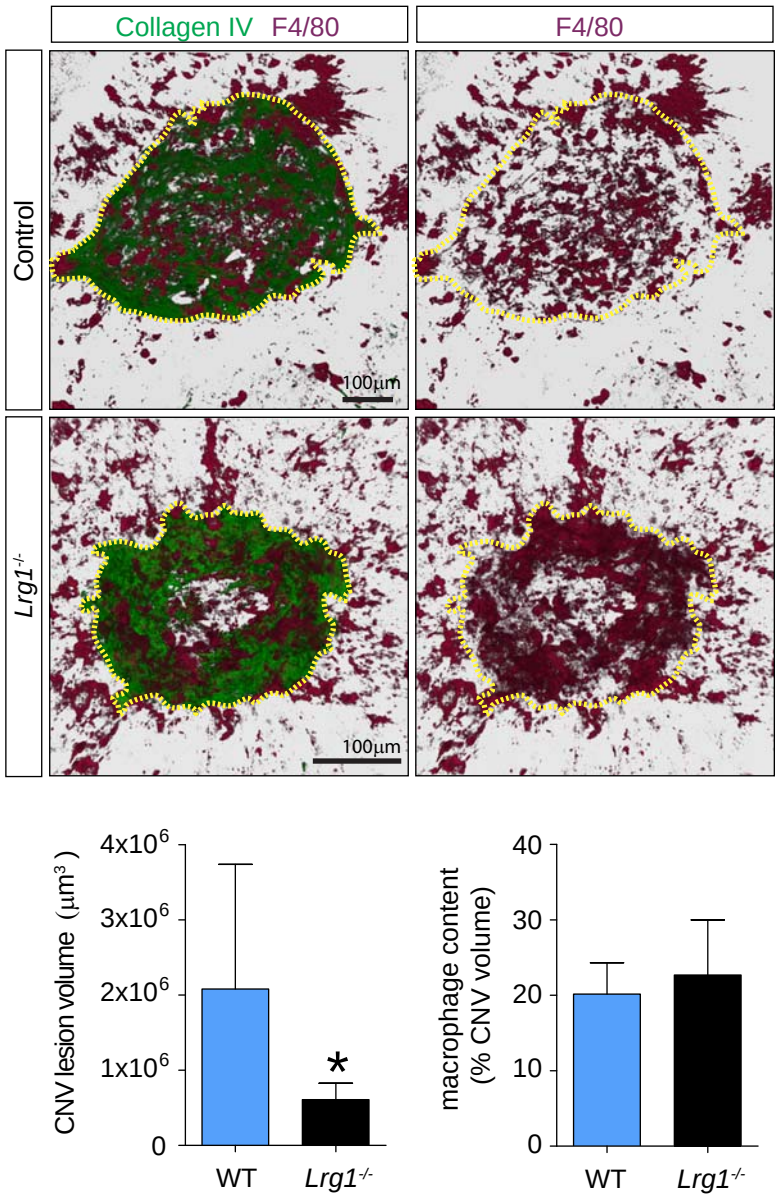

Supplementary Figure 20. Macrophage content of CNV lesions is similar in WT and *Lrg1*$^{-/-}$ mice. Representative Imaris reconstructed images of CNV lesions from WT control (top row) and *Lrg1*$^{-/-}$ (bottom row) mice. CNV lesion is stained for collagen IV (green) and macrophages stained for F4/80 (purple). The CNV lesion has been demarcated with a yellow dotted line. Below, histograms showing CNV lesion volume (left) and macrophage content (right) expressed as a percentage of CNV volume in WT and *Lrg1*$^{-/-}$ mice.

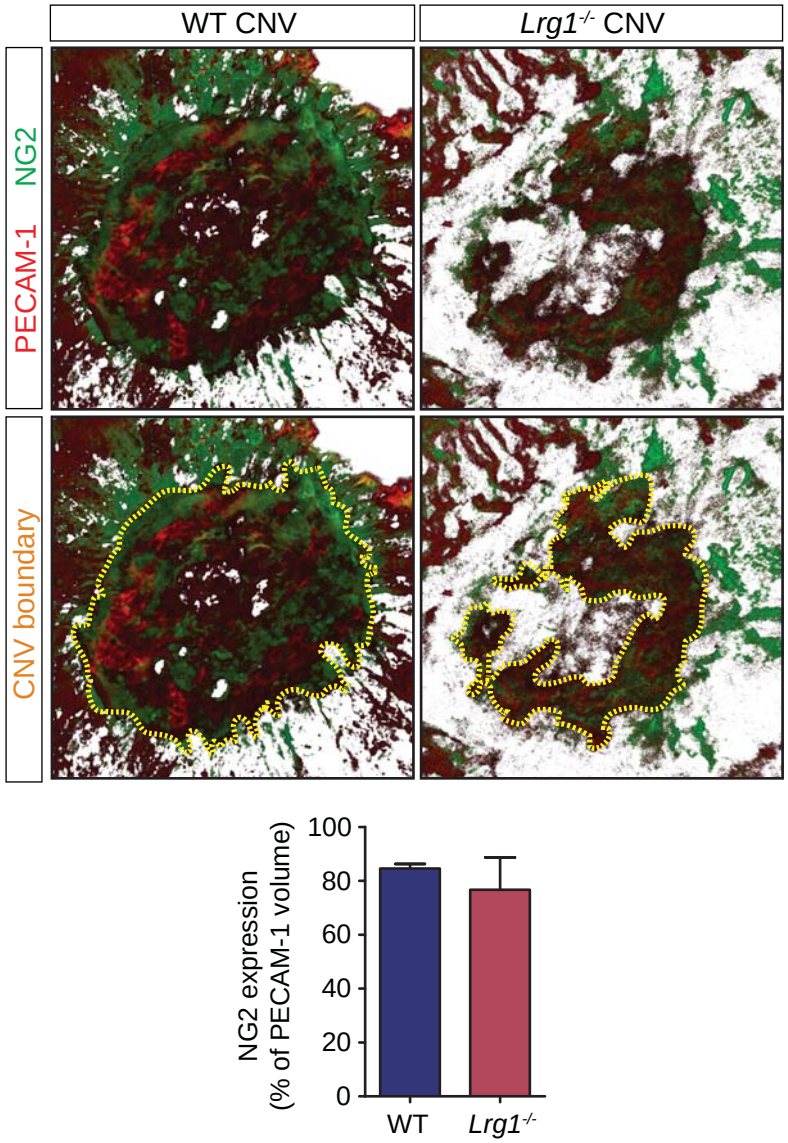

Supplementary Figure 21. CNV NG2 (pericyte) coverage is similar in WT and *Lrg1*$^{-/-}$ mice. Representative Imaris reconstructed images of CNV lesions from WT control (top left) and *Lrg1*$^{-/-}$ (top right) mice. CNV lesions are stained for PECAM-1 (red) and NG2 (green). Lower panels show delineation of CNV lesion (yellow dotted line). Below, histogram shows NG2 volume as a percentage of PECAM-1 volume in delineated CNV lesions in WT and *Lrg1*$^{-/-}$ mice. *n* = 3 per group.

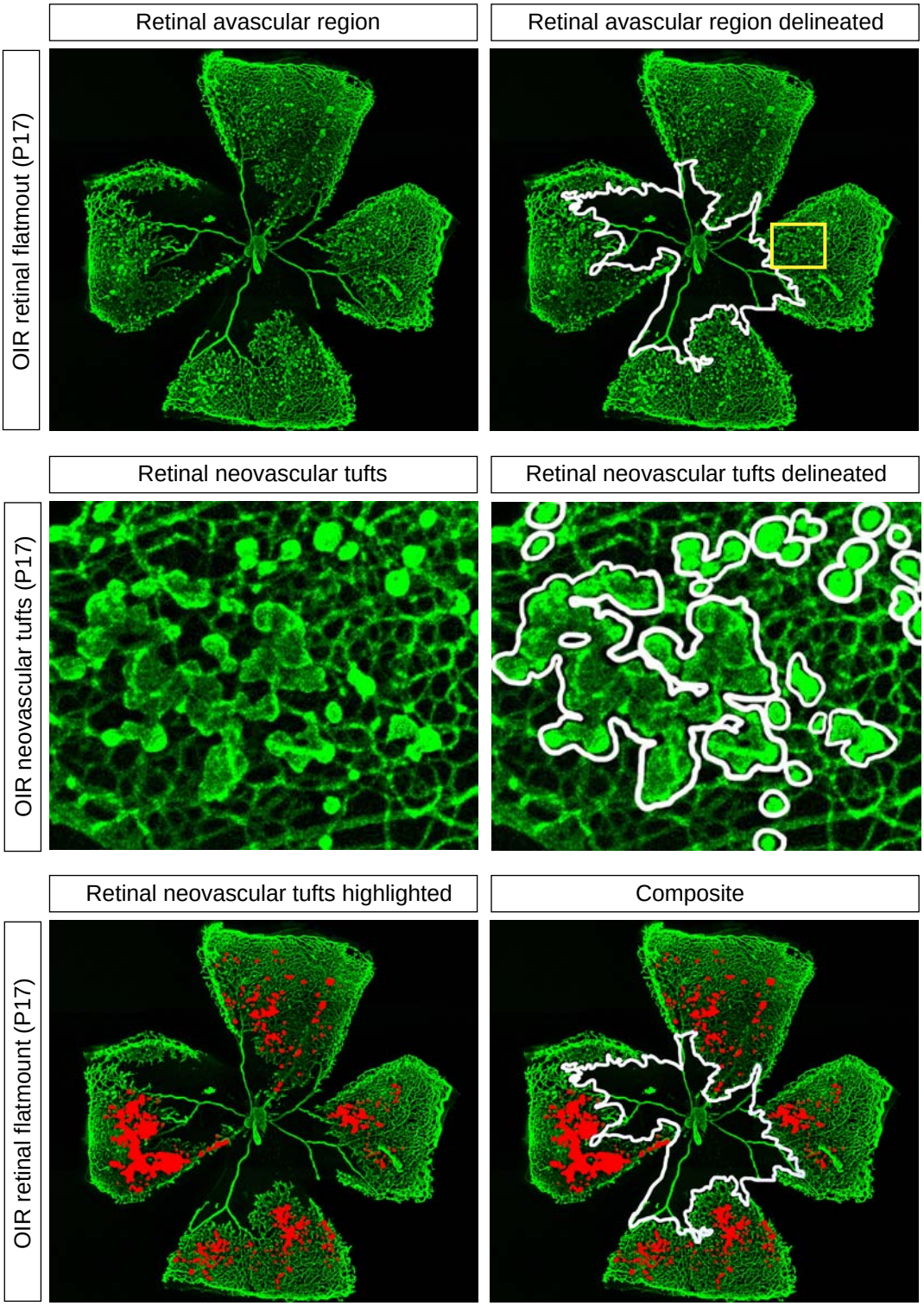

Supplementary Figure 22. Delineation of retinal avascular region and neovascular tufts in OIR for quantitative analysis. Top left shows a representative reconstructed (tile) flat mounted retina stained for PECAM-1 (green) from an OIR-induced mouse at P17. Top right illustrates the manual delineation of the vascular/avascular interface (white line) for area analysis. Middle left shows higher power image of yellow boxed area in top right to reveal the neovascular tufts. These are manually delineated (white line) for area analysis. Bottom left image shows artificially coloured neovascular delineated tufts (red) and the bottom right the composite showing neovascular tufts (red) and avascular region (white line).

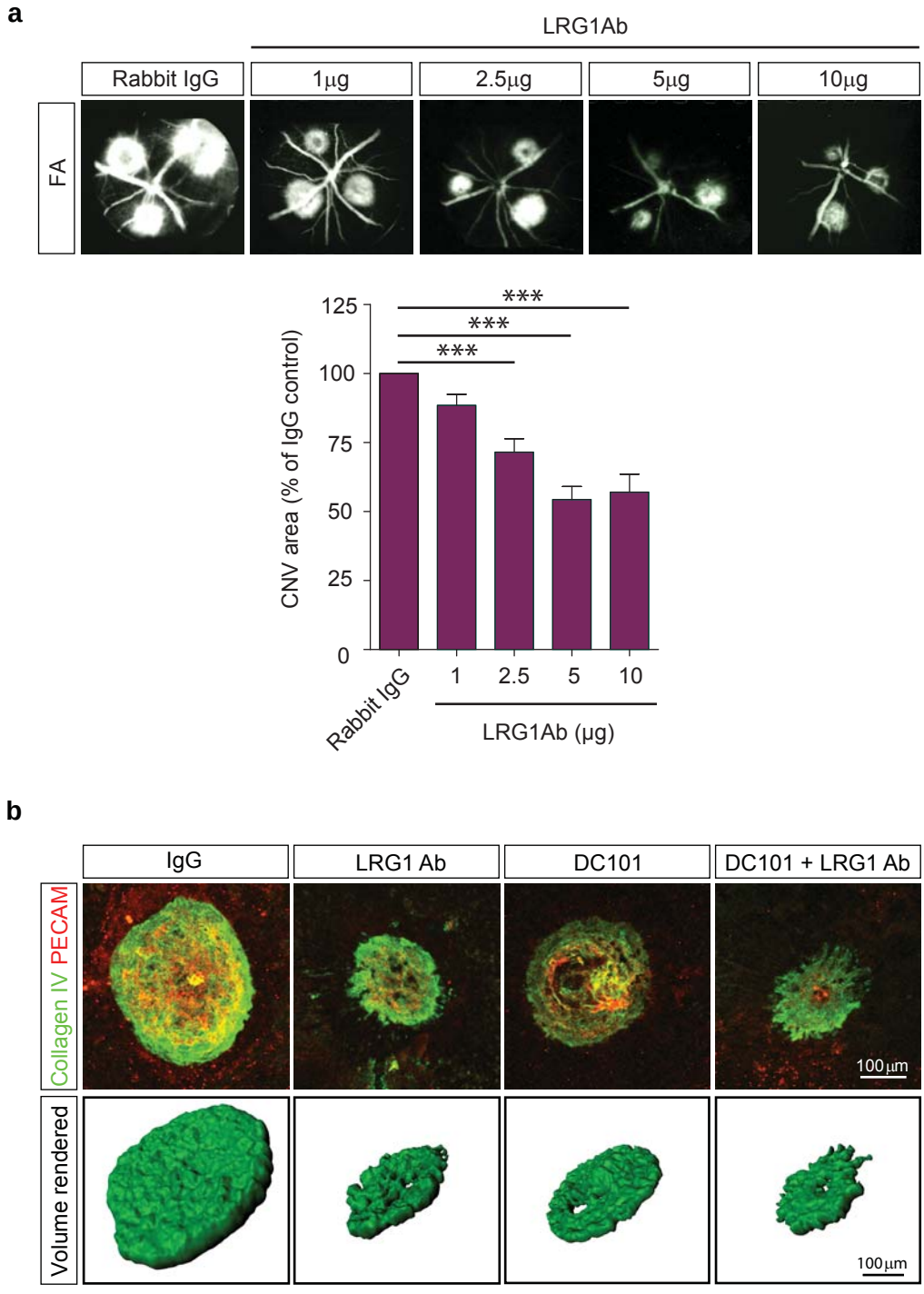

Supplementary Figure 23. Antibody blockade of LRG1 inhibits CNV lesion formation. **a,** Representative fluorescein angiographs of laser-induced CNV lesions from WT mice following intravitreal delivery of control IgG or LRG1 polyclonal antibody. The histogram shows a dose-dependent inhibition of CNV lesion area by the anti-LRG1antibody. Data analysed by one-way ANOVA (P = 0.0001) with significance from controls determined by Bonferroni's multiple comparison post-hoc analysis ($n \geq 15$ for each group, ***P<0.001). **b**, Representative confocal images (top) and 3D rendered equivalent reconstructions (bottom) of laser-induced CNV lesions from control, anti-LRG1 and anti-VEGFR2 (DC101) antibody treated WT mice. Whole mounts were stained for collagen IV (green) and PECAM-1 (red) and confocal Z stacks were 3D rendered using Imaris software.

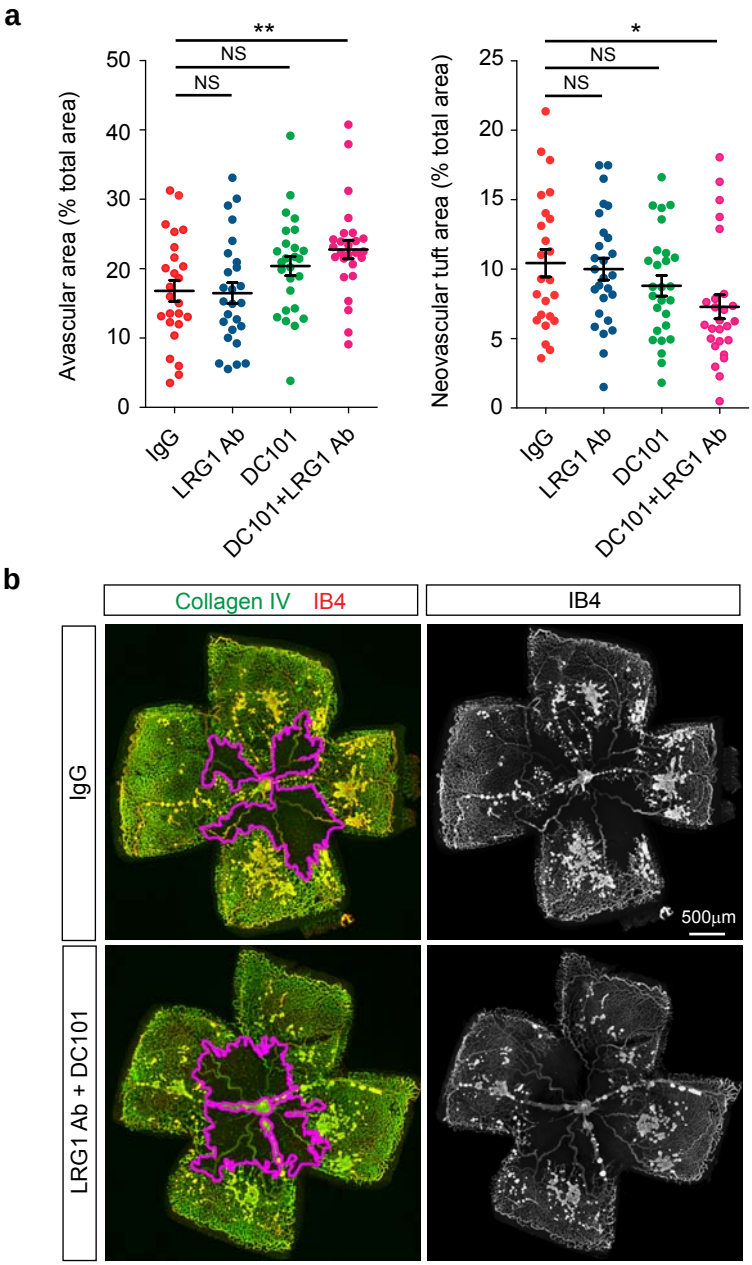

Supplementary Figure 24. Combined antibody blockade of LRG1 and VEGFR2 inhibits angiogenesis in OIR. a, Effect of anti-LRG1 blocking antibody (50mg/kg intraperitoneal in 100µl at P12 and P15), anti-VEGFR2 blocking antibody (DC101, 12.5mg/kg intraperitoneal at P12 and P15) or a combination of the two, on retinal revascularisation and neovascular tuft formation. With these treatment regimens significant inhibition was only observed with combined therapy, reducing both revascularisation (**P <0.01, n ≥ 15 for each group) and neovascular tuft formation (*P<0.05; n ≥ 15 for each group). One-way ANOVA (P = 0.0002) with significance from controls determined by Bonferroni's multiple comparison post-hoc analysis. **b**, Representative images of OIR from IgG control and anti-LRG1/DC101 treated mice. Whole mounts were stained for collagen IV (green) and isolectin B4 (red). Avascular region at day P17 (5 days post hyperoxia) is delineated by the magenta line. Neovascular tufts are more clearly observed as brighter regions on the greyscale images.

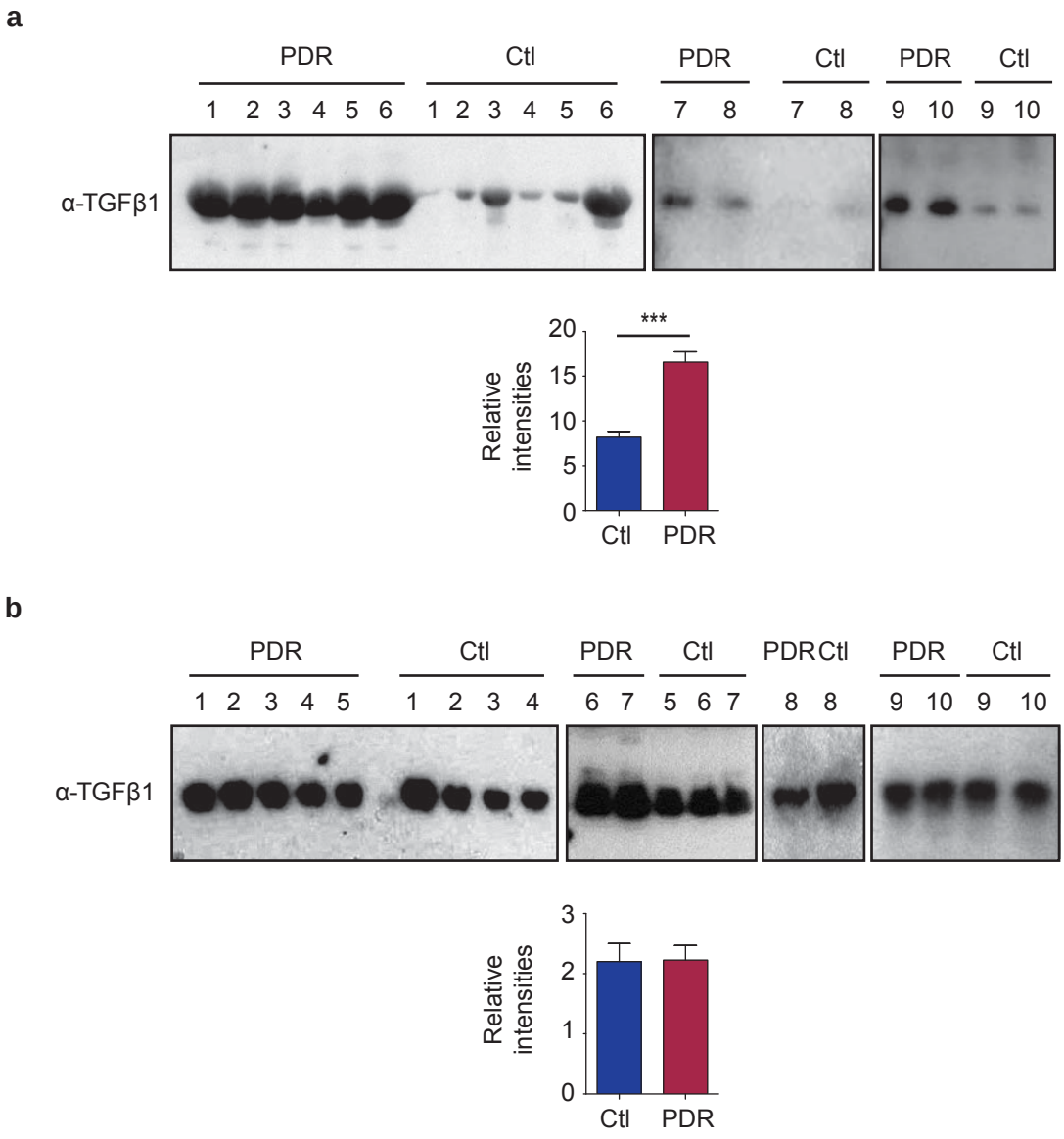

Supplementary Figure 25. TGFß1 is increased in the vitreous of patients with proliferative diabetic retinopathy. a, Western blots of vitreal TGFß1 from ten patients with proliferative diabetic retinopathy (PDR) and ten non-PDR controls (patients with epiretinal membranes). Quantitative analysis shows a significant increase of TGFß1 in PDR patients (***P<0.001). **b**, No significant difference in plasma TGFß1 protein level was observed between PDR and non-PDR control patients. Total vitreous/plasma protein was normalized before western blotting as shown by Coomassie blue staining of the SDS-PAGE gel in Supplementary figure 5. The TGFß1 protein level was determined by relative intensities against the total protein in vitreous /plasma using Image J. All values represent means ± s.e.m. Significance determined by Student's t-test (***P<0.001).

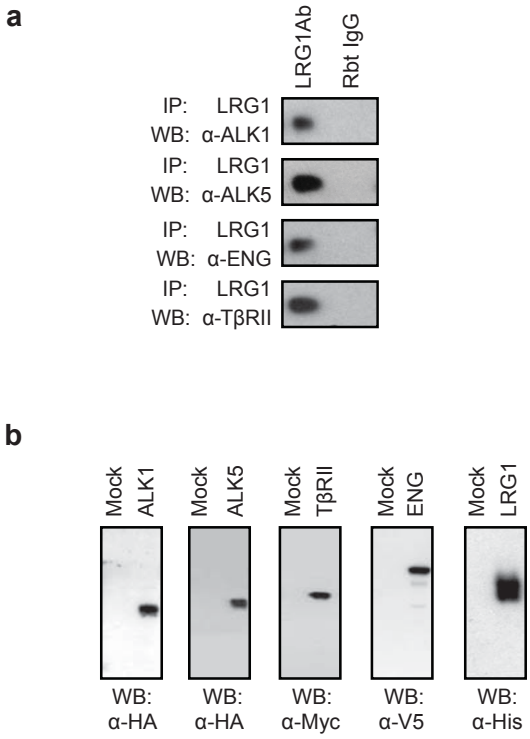

Supplementary Figure 26. Binding of LRG1 to TGFβ receptors and generation of peptide-tagged LRG1 and TGFβ receptor extracellular domains. a, Western blots showing that immunoprecipitation of LRG1 with polyclonal rabbit antibody from HUVEC lysates co-immunoprecipitates the TGFβ receptors TβRII, ALK1, ALK5 and endoglin (ENG). (Representative of $n \geq 3$ for each assay). **b**, Western blot of peptide-tagged recombinant extracellular domains of TGFβ receptors TβRII (Myc-tagged), ALK1 (HA-tagged), ALK5 (HA-tagged) and ENG (V5-tagged) and His-tagged LRG1 in transfected HEK 293 cell medium. (Representative western blots; $n \geq 3$ for each experiment).

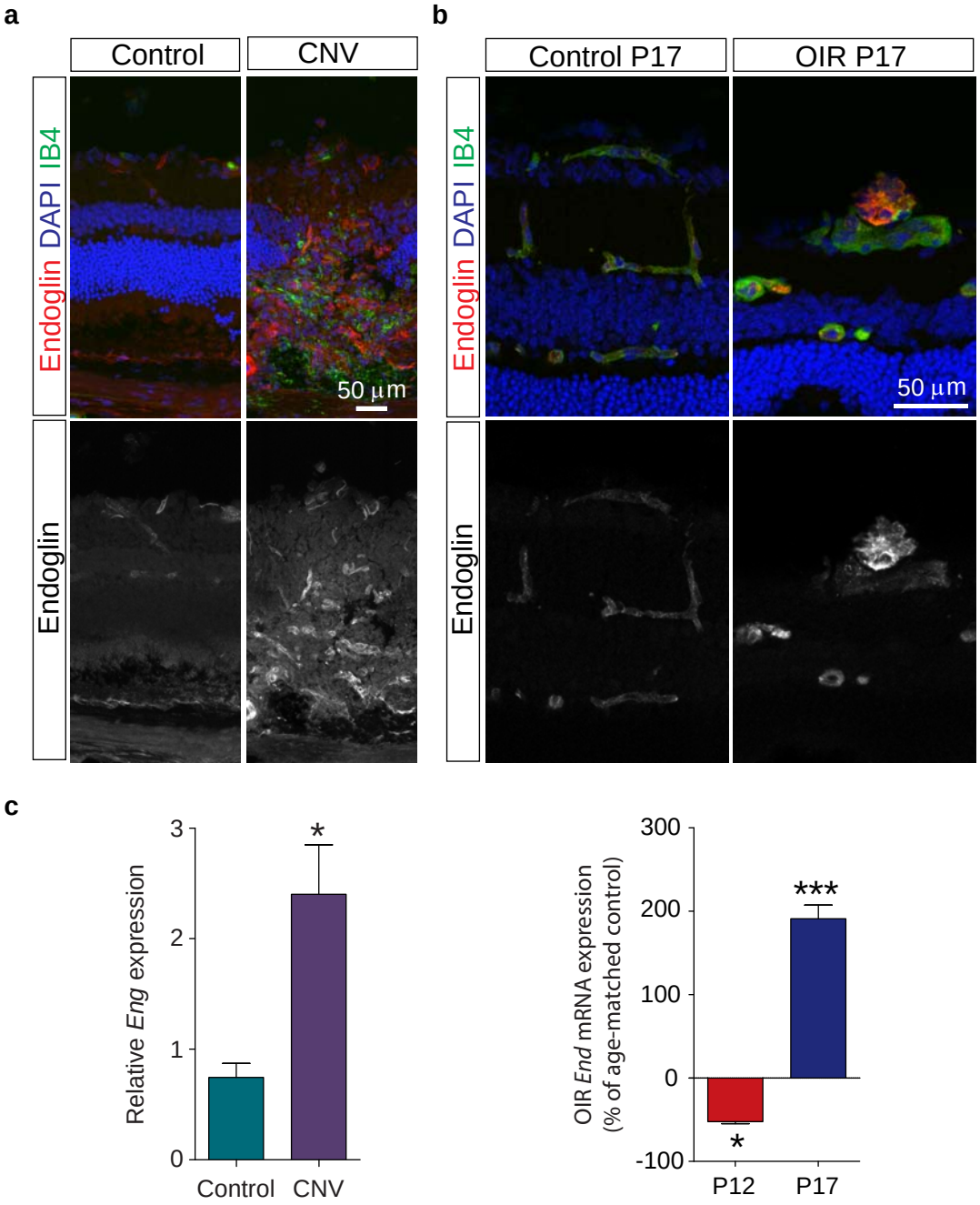

Supplementary Figure 27. Endoglin expression is upregulated in CNV and OIR neovascularisation. a, Representative immunohistological retinal sections of control (top left hand panel) and CNV lesion (top right hand panel) stained for endoglin (red), isolectin B4 (green) and nuclei (DAPI, blue). Lower panels show endoglin channel only. **b**, Representative immunohistological retinal sections of P17 control (top left hand panel) and P17 OIR lesion (top right hand panel) stained for endoglin (red), isolectin B4 (green) and nuclei (DAPI, blue). Lower panels show endoglin channel only. **c**, Histograms showing *Eng* mRNA relative to *Gapdh* mRNA in control and CNV retina (left) and relative to untreated age-matched WT control mice in OIR at P12 and P17. **P*<0.05; ****P*<0.001; *n* = 3 for each group.

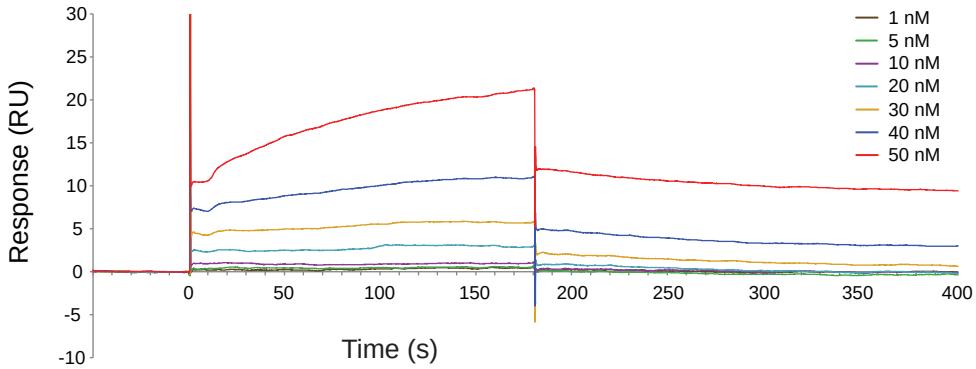

Supplementary Figure 28. Surface plasmon resonance analysis of LRG1-ENG binding. Real-time binding and dissociation assay was performed to determine binding kinetics of the ectodomain of ENG to LRG1 using Biacore T200. The GST tagged ectodomain domain of ENG (GST-ENG) was passed over LRG1 covalently immobilized to a CM5 sensor chip at increasing concentrations (0-50 nM). An association time of 3 minutes and a dissociation time of 5 minutes were used and the chip was regenerated between each concentration of GST-ENG. The binding curves show RU (Response Unit) as a function of time. The sensograms show a dose-dependent binding of ENG-GST to LRG1 after subtracting the background. GST on its own showed no binding to LRG1. Data provided an affinity rate constant (K_D) of 2.9 μM, an association rate constant (K_a) of 4.9 x 10^2 $M^{-1}s^{-1}$ and a dissociation rate constant (K_d) of 1.4 x 10^{-3} s^{-1}.

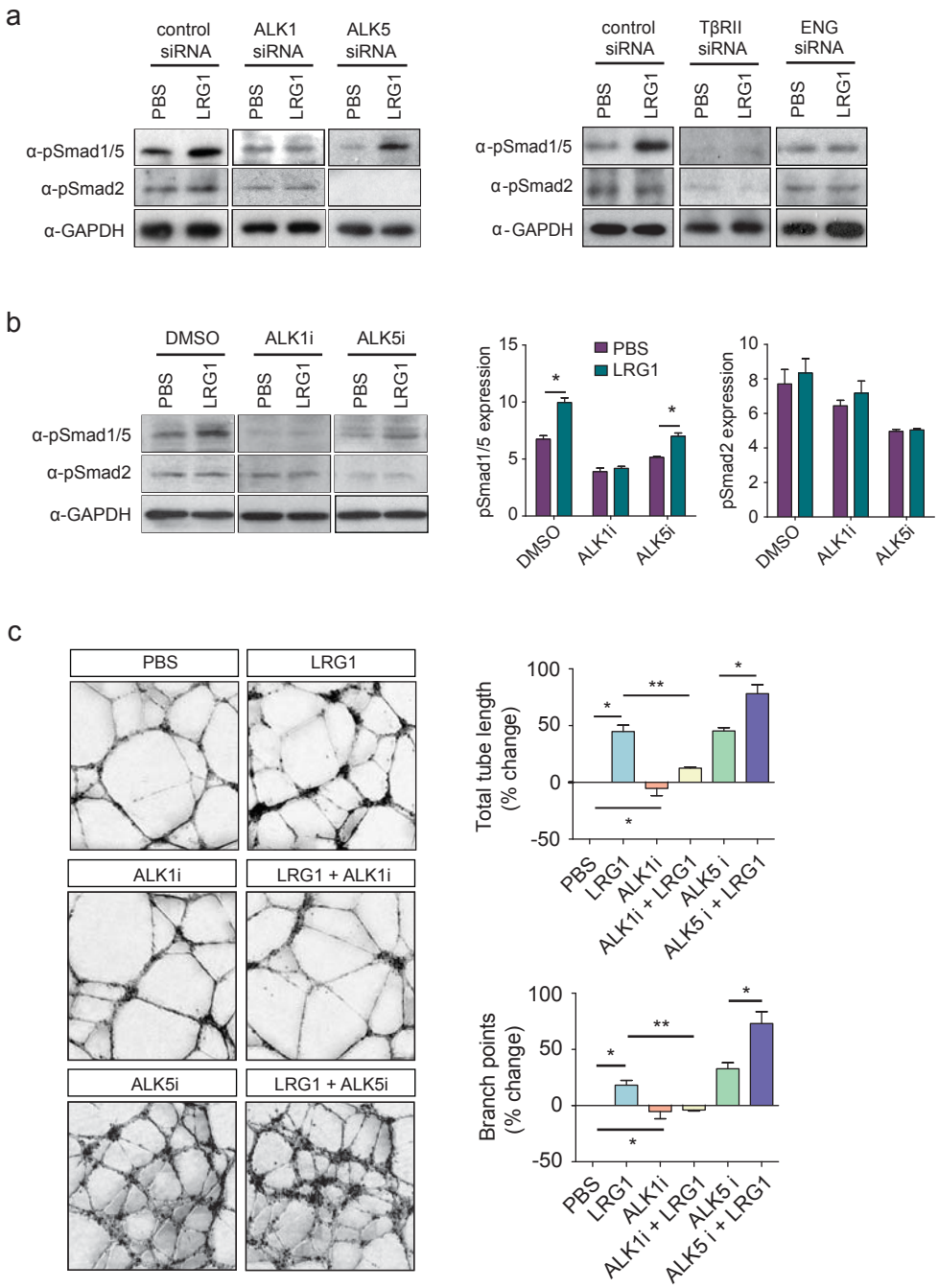

Supplementary Figure 29. Inhibition of ALK1, but not ALK5, inhibits LRG1-mediated Smad1/5 phosphorylation and HUVEC tube and branch formation. a, Western blot examples of siRNA knockdown of ALK1, ALK5, TβRII or ENG in HUVEC on LRG1-induced Smad1/5 and Smad2 phosphorylation. Knockdown of ALK1, TβRII and ENG, but not ALK5, results in prevention of LRG1-induced Smad1/5 phosphorylation. See Figure 5 for semi-quantification. ($n \geq 3$). **b,** The ALK1 inhibitor LDN193189 (ALK1i) inhibits LRG1-induced phosphorylation of Smad1/5 but has no effect on Smad2 phosphorylation. Conversely, the ALK5 inhibitor SB43152 (ALK5i) has little effect on LRG1-induced Smad1/5 phosphorylation. Histograms show semi-quantification of Smad phosphorylation relative to GAPDH ($n \geq 3$; *P<0.05). **c,** Representative images of the HUVEC Matrigel assay showing inhibition of LRG1-mediated tube and branch formation with the ALK1 inhibitor LDN193189 (ALK1i) but not the ALK5 inhibitor SB43152 (ALK5i). Histograms show tube length and branch formation under the different conditions. (*P<0.05; **P<0.01; n=3 independent assays). All values represent means ± s.e.m.

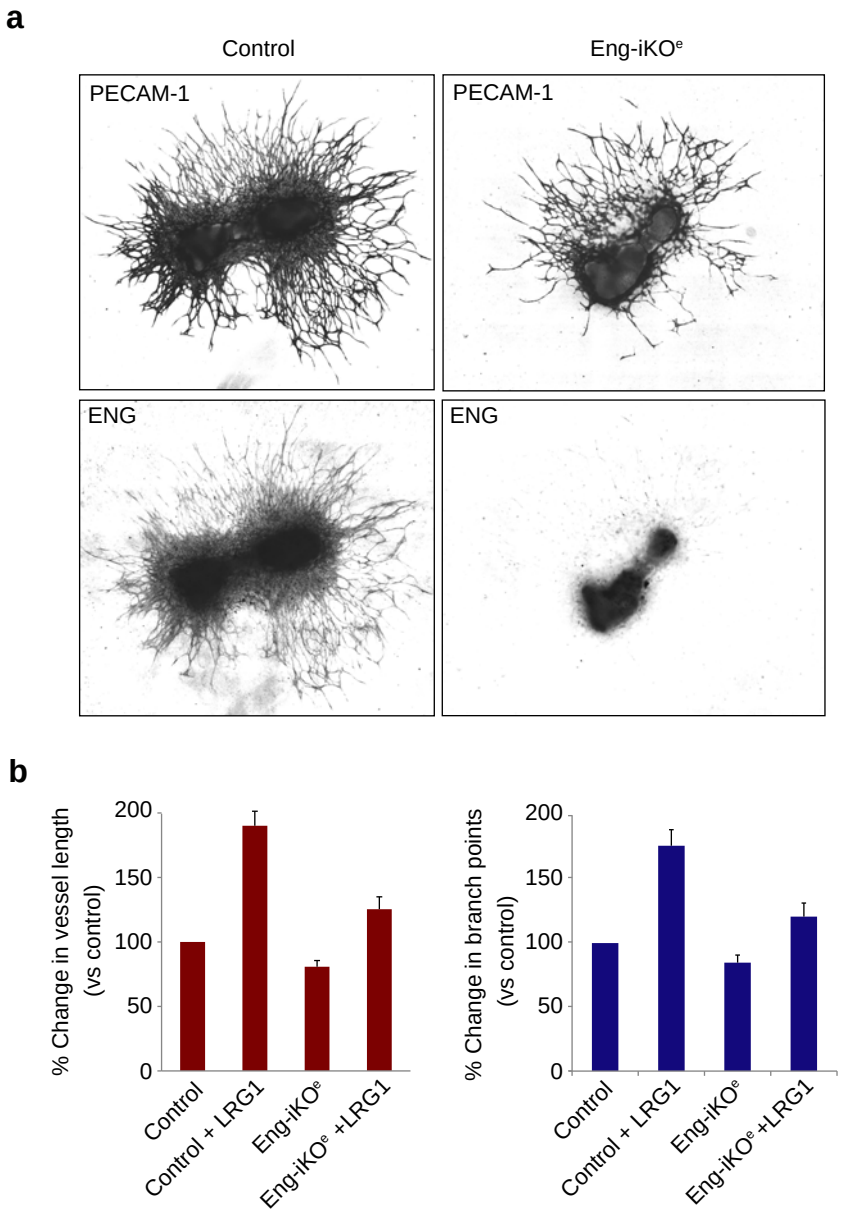

Supplementary Figure 30. Depletion of endothelial ENG expression in metatarsal angiogenesis assay and its effect on vessel length and branching. a, Representative images of PECAM-1 and ENG staining of 4OH-tamoxifen treated metatarsals from *Eng*$^{fl/fl}$ (control) and *Cdh5(PAC)-CreERT2;Eng*$^{fl/fl}$ (Eng-iKO^{e}) mice showing ENG depletion in the latter. **b,** Percentage change in metatarsal vessel length and branching following 4OH-tamoxifen treatment of *Eng*$^{fl/fl}$ metatarsals (control) and *Cdh5(PAC)-CreERT2;Eng*$^{fl/fl}$ metatarsals (Eng-iKO^{e}).

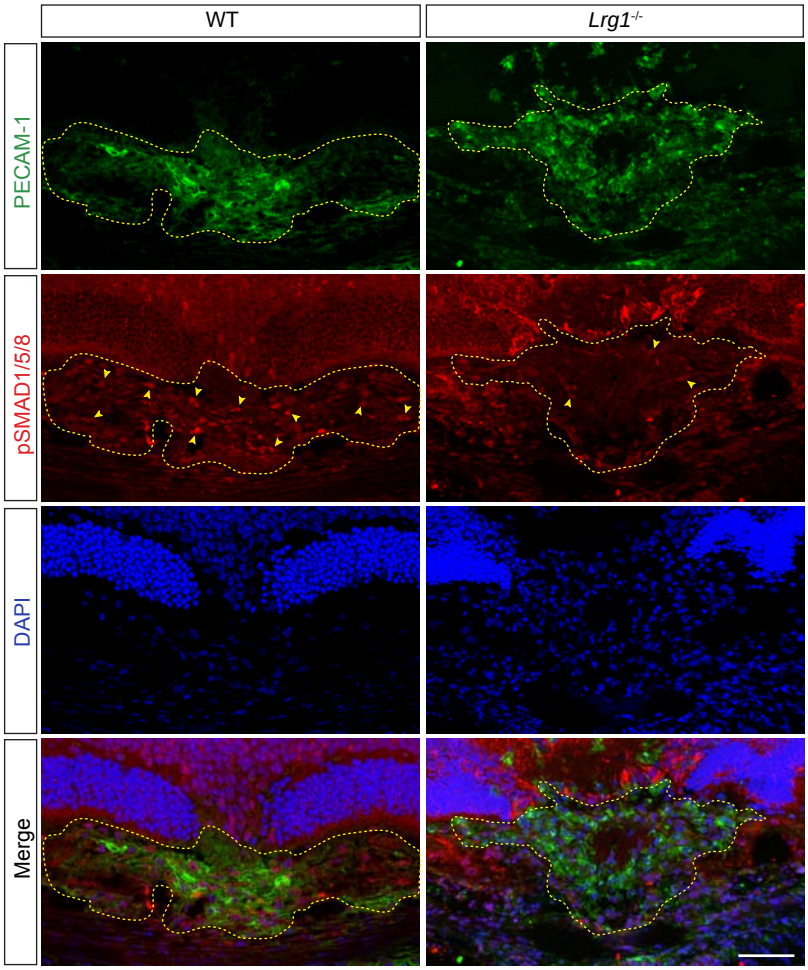

Supplementary Figure 31. pSmad1/5/8 expression in CNV. Representative immunohistological section of CNV lesions in wild type (WT) and Lrg1 knockout (*Lrg1*$^{-/-}$) mice stained for PECAM-1 (green) to reveal endothelial cells and phosphorylated Smad1/5/8 (red). The boundary of the CNV lesion has been demarked by a dotted yellow line. Fewer phospho-Smad1/5/8 cells were observed in the CNV lesion in the *Lrg1*$^{-/-}$ mice. Nuclei were stained with DAPI (blue). Scale bar 50μm.

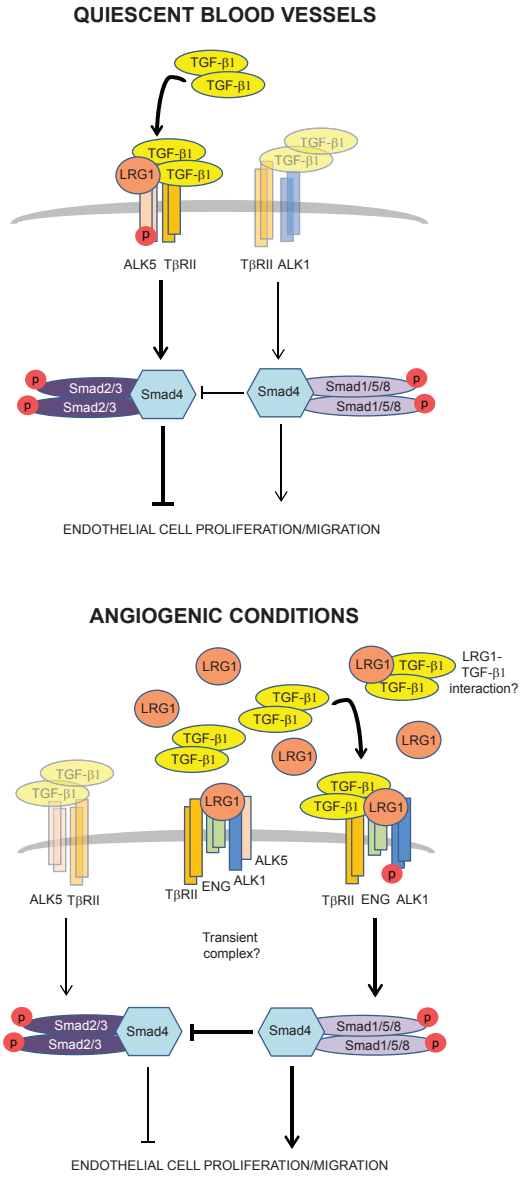

Supplementary Figure 32. Proposed model of LRG1 mediated TGFβ1 endothelial cell signalling. Under resting conditions TGFß1 signalling in endothelial cells is predominantly via the TβRII-ALK5-Smad2/3 pathway which maintains vascular homeostasis. During pathogenic angiogenesis there is an increase in LRG1 and ENG production. The interaction between LRG1 and TGFβ1 may facilitate more efficient ENG/TβRII/ALK1 receptor complex formation resulting in a switch in TGFβ1 signalling to the ALK1-Smad1/5/8 pathway and a pro-angiogenic transcriptional response. LRG1/ENG/TβRII/ALK1/ALK5 may form an intermediate/transient complex to allow the efficient phosphorylation of ALK1 but in the presence of TGFβ1, LRG1/ENG/ALK1/TβRII predominates.